



Promising antioxidant and anticancer (human breast cancer) oxidovanadium(IV) complex of chlorogenic acid. Synthesis, characterization and spectroscopic examination on the transport mechanism with bovine serum albumin



Luciana G. Naso^a, María Valcarcel^b, Meritxell Roura-Ferrer^b, Danel Kortazar^b, Clarisa Salado^b, Luis Lezama^c, Teofilo Rojo^c, Ana C. González-Baró^a, Patricia A.M. Williams^a, Evelina G. Ferrer^{a,*}

^a Centro de Química Inorgánica (CEQUINOR, CONICET, UNLP), Departamento de Química, Facultad de Ciencias Exactas, Universidad Nacional de La Plata, 47 y 115, C.C. 962 (B1900AVV), 1900 La Plata, Argentina

^b INNOPROT, Parque Tecnológico de Bizkaia, Edif. 502-1°, Derio, Spain

^c Departamento de Química Inorgánica, Facultad de Ciencia y Tecnología, Universidad del País Vasco, Apdo 644, 48080 Bilbao, Spain

ARTICLE INFO

Article history:

Received 12 August 2013

Received in revised form 10 February 2014

Accepted 11 February 2014

Available online 6 March 2014

Keywords:

Albumin interaction
Anticancer activity
Antioxidant activity
Chlorogenic acid
Oxidovanadium(IV)

ABSTRACT

A new chlorogenate oxidovanadium complex ($\text{Na}[\text{VO}(\text{chlorog})(\text{H}_2\text{O})_3] \cdot 4\text{H}_2\text{O}$) was synthesized by using Schlenk methodology in the course of a reaction at inert atmosphere in which deprotonated chlorogenic acid ligand binds to oxidovanadium(IV) in a reaction experiment controlled via EPR technique and based in a species distribution diagram. The compound was characterized by FTIR, EPR, UV–visible and diffuse reflectance spectroscopies and thermogravimetric, differential thermal and elemental analyses. The ligand and the complex were tested for their antioxidant effects on DPPH[•] (1,1-diphenyl-2-picrylhydrazyl radical), ABTS^{•+} (radical cation of 2,2'-azinobis(3-ethylbenzothiazoline-6-sulfonic acid) diammonium salt), $\text{O}_2^{\cdot-}$, OH[•] and ROO^{\cdot} radicals and their cytotoxic activity on different cancer cell lines (SKBR3, T47D and MDAMB231) and primary human mammary epithelial cells. The complex behaved as good antioxidant agent with strongest inhibitory effects on $\text{O}_2^{\cdot-}$, OH[•] and ROO^{\cdot} radicals and exhibited selective cytotoxicity against SKBR3 cancer cell line. Albumin interaction experiments denoted high affinity toward the complex and its calculated binding constant was indicative of a strong binding to the protein. Based on this study, it is hypothesized that $\text{Na}[\text{VO}(\text{chlorog})(\text{H}_2\text{O})_3] \cdot 4\text{H}_2\text{O}$ would be a promising candidate for further evaluation as an antioxidant and anticancer agent.

© 2014 Elsevier Inc. All rights reserved.

1. Introduction

In recent years, non-flavonoid compounds containing catechol groups in their molecules became of increasing interest due to their multiple biological and pharmacological functions. Hydroxycinnamic acids, as caffeic, ferulic, sinapic and p-coumarin acid are present in vegetables and fruits such as blueberries, grapes, bran, apples, lettuce, broccoli and spinach [1,2]. Chlorogenic acid (3-O-caffeoyl-D-quinic acid, $\text{C}_{16}(\text{H}_2\text{O})_9$) (Fig. 1) is an ester formed from caffeic and quinic acids. It contains both aliphatic and aromatic groups and it is one of the major polyphenolic components present in coffee seeds and tobacco leaves [3,4]. Like other polyphenols present in the diet, chlorogenic acid showed antioxidant properties [5], such as antioxidative effects during autoxidation of triacylglycerols of sunflower oil [5], protective effect on blood granulocytes from oxidative stress [6], scavenging ability of N_2O_3 , organic free radicals, HOCl, $\text{O}_2^{\cdot-}$, OH[•], ONOO⁻ and peroxy

radical/s [7]. It also produced a protective effect against ischemia/reperfusion (I/R) injury [8]. It has also been suggested that this compound eliminated radicals and increased the resistance of LDL (low density lipoprotein) to inhibit lipid peroxidation and DNA damage. In vivo, when added to the diet, it inhibited chemically induced carcinogenesis in the large intestine, liver and tongue in rats and hamsters [9]. Various phenolic acids showed antibacterial activity against Gram-positive (*Staphylococcus aureus* and *Listeria monocytogenes*) and Gram-negative bacteria (*Escherichia coli* and *Pseudomonas aeruginosa*) [10]. In this context, chlorogenic acid behaved as natural scavenger for hypochlorous acid [11] and as HIV-1 RNase inhibitor [12]. Anti-proliferative effect on HepG2 cells using *Rhizoma Smilacis Chinae* extracts (30% chlorogenic acid component) [13], apoptosis induction of Bcr–Abl⁺ chronic myeloid leukemia (CML) cell lines and inhibition of Bcr–Abl phosphorylation in clinical leukemia samples have been investigated [9].

The biological functions performed by oxidovanadium(IV) species have gained increasing interest in inorganic salts as oxidovanadium(IV) sulfate produced normalization of the glucose

* Corresponding author. Tel./fax: +54 221 4259485.
E-mail address: evelina@quimica.unlp.edu.ar (E.G. Ferrer).

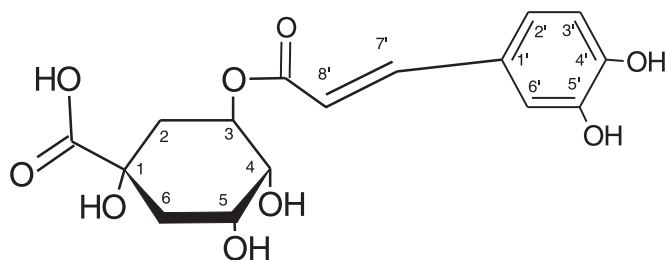


Fig. 1. Structure of chlorogenic acid (3-O-caffeoyl-D-quinic acid, $C_{16}(H_2O)_9$).

levels in STZ-D (streptozotocin-diabetic) rats while in other oxidovanadium complexes the lowering effect found was $[VO(mal)_2] > [VO(cysm)_2] > [VO(tar)_2] > [VO(sal)_2] > [VO(ox)_2]$ (cysm = cysteine methyl ester, ox = oxalate, mal = malonate, sal = salicylaldehyde, tar = $-(+)$ -tartarate) when the dose was of 10 mg V/kg body weight [14]. Besides their best known insulinomimetic behavior, vanadium compounds have recently come out as antiparasitic agents denoting *anti-T. cruzi* (*antitrypanosomal*) activity, and acting against *Serratia species*, *Micrococcus luteus* and *Proteus vulgaris*. Enzyme inhibition action has also been widely reported to be associated to several pathologies [15] as well as their behavior as potent catalyst.

In recent years, scientists began to pay more attention to the antitumor effects of vanadium compounds [16–18]. Several oxidovanadium complexes were tested as anticancer agents. Among them, those having ligands such as cyclopentadienyl or phenanthroline, including the well known METVAN active compound [bis(4,7-dimethyl-1,10-phenanthroline) oxidovanadium(IV) sulfate]; NSAIDs (non-steroidal antiinflammatory drugs), curcumin and bis-acetylacetonate [14]. Focusing on breast cancer, Bishayee et al. [16] reported the dietary use of vanadyl sulfate and ammonium monovanadate and also the employment of vanadocene dichloride (VDC) in the treatment of progressed stages of fluid Ehrlich ascites tumor (EAT), a spontaneous breast carcinoma in mice. Other tests were performed on BT-20 breast cancer cells by using oxidovanadium compounds including *mono* and *bis* 1,10-phenanthroline as ancillary ligands [19].

For several years the objective of our investigations has been the study of the enhancement of the anticarcinogenic activity of the flavonoids upon complexation with oxidovanadium(IV) cation. For this reason the antiproliferative effects against normal (MC3T3E1) and tumoral (UMR106) osteoblast-like cells were investigated and compared with that of free ligands and free $V^{(IV)}O_2^{2+}$ species [20–23]. Recently, in collaboration with INNOPROT we begin to explore the activity of our compounds in breast cancer cell lines. We have found in the literature only few vanadium complexes that have been tested for breast cancer cell lines: (i) some vanadium(V) complexes [24–26] and also the well known BMOV (bis(maltolato) oxidovanadium) were tested on MCF-7 cell line by using a polymer-based drug delivery system; (ii) other experiments were performed on BT-20 cancer cells with oxidovanadium compounds including *mono* and *bis* 1,10-phenanthroline as ancillary ligands [19] and (iii) METVAN ((4,7-dimethyl-1,10-phenanthroline) sulfatooxidovanadium(IV)) was tested on MDA-MB-231 cancer cell lines giving an IC_{50} value of $11.6 \pm 1.8 \mu M$ [27].

Hitherto, not many vanadium metal complexes were found to be active in terms of restraining the reproduction of breast cancer cells. Based on the previous considerations, we are currently interested in the investigation of the interaction of simple oxidovanadium species with ligand groups bearing pharmacological activity, particularly those with antitumor ability. As part of our current studies we prepared and characterized an oxidovanadium complex with chlorogenic acid. We investigated the antioxidant and antitumoral activities including some possible mechanisms of action and we evaluated the albumin transport ability by studying its interaction using spectroscopic methodologies.

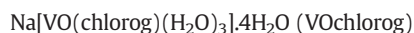
2. Materials and methods

2.1. Reagents and instrumentation

Chlorogenic acid (Fluka), oxidovanadium(IV) chloride (50% aqueous solution, Carlo Erba), and solid oxidovanadium(IV) sulfate pentahydrate (Merck) were used as supplied. Bovine serum albumin (BSA) (A-6003, essentially fatty acid-free) was obtained from Sigma Chemical Company (St. Louis, MO) and used as supplied. Corning or Falcon provided tissue culture materials. Trypsin and EDTA were purchased from Gibco (Gaithersburg, MD, USA), and fetal bovine serum (FBS) was from GibcoBRL (Life Technologies, Germany). All other chemicals used were of analytical grade. Elemental analysis for carbon and hydrogen was performed using a Carlo Erba EA1108 analyzer. Vanadium content was determined by the tungstophosphovanadic method [20]. Thermogravimetric analysis (TGA) was performed with Shimadzu systems (models TG-50), working in an oxygen flow of 50 mL min^{-1} and at a heating rate of $10 \text{ }^\circ\text{C min}^{-1}$. Sample quantities ranged between 10 and 20 mg. UV–vis spectra determinations were recorded with a Hewlett-Packard 8453 diode-array spectrophotometer. The diffuse reflectance spectrum was recorded with a Shimadzu UV-300 spectrophotometer, using MgO as a standard. Infrared spectra were measured with a Bruker IFS 66 FTIR spectrophotometer from 4000 to 400 cm^{-1} using the KBr pellet technique. A Bruker ESP300 spectrometer operating at the X-band and equipped with standard Oxford Instruments low-temperature devices (ESR900/ITC4) was used to record the spectrum of the complex at room temperature in the solid state. Anisotropic X-band EPR spectra of frozen solutions were recorded at 140 K, after addition of 5% DMSO to ensure good glass formation. A computer simulation of the EPR spectra was performed using the program WINEPR SimFonia [20] (version 1.25, Bruker Analytische Messtechnik, 1996). Fluorescence spectra were obtained using a Perkin Elmer (Beaconsfield, UK) LS-50B luminescence spectrometer equipped with a pulsed xenon lamp (half peak height less than 10 ns, 60 Hz), an R928 photomultiplier tube, and a computer working with FL WinLab.

2.2. Synthesis

The synthesis of the vanadium compound was performed under high-purity nitrogen atmosphere using standard Schlenk techniques. Solvents were saturated in dry nitrogen before use. The appropriate synthesis condition was followed by using EPR spectroscopy in order to circumvent oxidation process. Several M:L (metal:ligand) ratios were proved but they produced V(V) or V(III) species or other products that cannot be identified and/or purified. Finally, the solution speciation profiles (see below) were also taken into consideration to select the stoichiometry of the solid complex.



A quantity of 0.125 mmol of chlorogenic acid (chlorog) was dissolved in 3 mL of a methanol: water (0.5:3) proportion on which an appropriate volume of an aqueous solution of $VOCl_2$ (50%) was added to obtain a 1:1 (L:M) ratio. The resulting mixture was stirred for 15 min and the pH was adjusted to a value of 5 with a 1 M NaOH solution. After this time, addition of isopropyl alcohol in excess produced a violet precipitate which was filtered by suction and washed several times with the same alcohol. Finally it was oven-dried at $60 \text{ }^\circ\text{C}$. Yield: 50%. *Anal.* $C_{16}H_{29}O_{17}VNa$. *Calcd for:* C, 33.8, H, 5.1, V, 9.0; Na, 4.1%. *Exp:* C, 33.5, H 5.2, V, 9.2; Na, 4.2%.

The UV–vis spectrum obtained by dissolving the VOchlorog complex ($2.3 \times 10^{-3} \text{ M}$) in water showed two absorption bands located at 555 nm ($3dxy \rightarrow 3d_{x^2-y^2}$), $\epsilon = 60.20 \text{ M}^{-1} \text{ cm}^{-1}$ and 864 nm ($3dxy \rightarrow 3dxz$, $3dyz$, $\epsilon = 42.04 \text{ M}^{-1} \text{ cm}^{-1}$). The complex remains stable in DMSO and water solutions (no changes were observed in the UV–vis spectra) for at least 60 min (the manipulation time for biological studies was

15 min). TGA: in the thermal decomposition of VOchlorog two stages were observed: (i) the first stage fits well with the loss of 4 water molecules (range 20–120 °C, $\Delta W_{exp.} = 12.40\%$; $\Delta W_{calcd.} = 12.69\%$) and (ii) the second stage reasonably agrees with the loss of 3 water-coordinated molecules (range 120–200 °C, $\Delta W_{exp.} = 10.20\%$; $\Delta W_{calcd.} = 9.52\%$). The final residue obtained at 800 °C was characterized by infrared spectroscopy as NaVO_3 . The weight of the final residue was 21.11% in agreement with the theoretical value (21.51%). Diffuse reflectance spectrum showed a well-defined band at 483 nm and a broad band whose maximum appeared at 750 nm (with components at 689 nm and 764 nm, obtained by curve fitting). These bands displayed the typical pattern of three bands characteristic of diol groups–oxidovanadium(IV) coordination [28].

2.3. Potentiometric titrations

The EMF measurements were performed with a Mettler Toledo DL50 Graphics pH meter. Volume of titrated aliquots was always 25 mL. $\text{VOSO}_4 \cdot 5\text{H}_2\text{O}$ was used without further purification and dried at 60 °C until constant weight before preparing the solutions. The “formula weight” was re-calculated ($\text{VOSO}_4 \cdot 4.84\text{H}_2\text{O}$, f.w. = 250.12) on the basis of a thermogravimetric analysis. NaCl was dried until constant weight and stored over CaCl_2 . All solutions were made in boiled tridistilled water. The solutions were freshly prepared prior to their use. Diluted solutions of HCl (Merck p.a.) were standardized against TRISMA-base (hydroxymethyl aminomethane). Diluted NaOH solutions were prepared from a saturated NaOH solution and standardized against potassium biphtalate and contrasted with the HCl standard. Cell compartments were kept at 25 ± 0.1 °C with circulating water from a thermostated bath. The ionic strength was fixed at $[\text{Na}^+] = 0.150$ M with NaCl in the solutions. The glass electrode was calibrated separately in a solution with known $[\text{H}^+]$ before and after each titration.

2.3.1. L^3^-/H^+ system (*L*: chlorogenate anion, *H*₃*L*: chlorogenic acid)

Ligand solutions were titrated in the absence of metal to determine the dissociation constant values (pK_a). Two series of titrations were performed in different conditions:

- (a) Vessel: H_3L 5 mM/HCl 2.5 mM, burette: NaOH 10 mM (pH 2.7–11.0).
- (b) Vessel: H_3L 5 mM/HCl 5 mM, burette: NaOH 20 mM (pH 2.4–11.2).

2.3.2. $\text{L}^3^-/\text{V(IV)O}^{2+}/\text{H}^+$ system

In order to determine the formation constants of the $\text{L}^3^-/\text{V(IV)O}^{2+}/\text{H}^+$ system, further titrations of vanadium/ligand solutions were performed in the pH range 2.4–11. Different experimental conditions were used:

- (a) Vessel: H_3L 5 mM/oxidovanadium(IV) 2.5 mM/HCl 5 mM, burette: NaOH 30 mM.
- (b) Vessel: H_3L 5 mM/oxidovanadium(IV) 1.25 mM/HCl 5 mM, burette: NaOH 30 mM.

2.4. BSA interactions

2.4.1. Fluorescence measurements

BSA was dissolved in Tris–HCl (0.1 M, pH 7.4) buffer to attain a final concentration of 6 μM . Chlorogenic acid, V(IV)O^{2+} and the complex were added dropwise to the 6 μM BSA solution and left to rest to ensure the formation of a homogeneous solution and to obtain the desired concentration of 2–100 μM . For each sample and concentration, three independent replicates were performed. The measurements were carried out on a Perkin-Elmer LS-50B luminescence spectrometer (Beaconsfield, England) equipped with a pulsed xenon lamp (half peak height < 10 ns, 60 Hz), an R928 photomultiplier tube and a computer working with FL WinLab software. Both excitation and emission slits were set at 5 nm

throughout this study. BSA (6 μM) was titrated by successive additions of chlorogenic acid and the complex salt solution from 2.0 to 100.0 μM and the fluorescence intensity was measured (excitation at 280 nm and emission at 348 nm) at 25 °C. Three independent replicates of BSA solution and the corresponding complexes were determined.

FT-IR spectra: spectra of the freeze-dried powdered samples were collected under similar condition. Then, the absorbance values of the buffer solution were subtracted from the values of the protein solution to get the FT-IR spectra of the protein. All spectra were vector normalized in the whole range ($4000\text{--}500\text{ cm}^{-1}$) and were obtained after collecting and averaging 200 scans. In order to improve signal-to-noise ratio in FTIR spectra, Tris–HCl buffer, BSA 2% w/w solutions and the 0.5 mM solutions of VOCl_2 , chlorogenic and VOchlorog in BSA 2% w/w were lyophilized. As with other proteins, particularly globulins, FT-Raman spectra of protein solutions and freeze-dried powders are almost identical, therefore, freeze drying does not affect protein conformation as determined by FT-Raman spectroscopy [29]. This fact was taken into account during the procedure. All analyses were performed in three independent experiments, and the results were reported as averages of these replicates. Determination of secondary structure of BSA and the samples containing VOCl_2 , chlorogenic and VOchlorog in BSA was carried out on the basis of the procedure described by Byler and Susi [30]. The Amide I region ($1700\text{--}1600\text{ cm}^{-1}$) was used to investigate the secondary structure of BSA in a quantitative manner. The frequencies, the number of peaks to be fitted, and the half-width of each peak to start a least square iterative curve-fitting procedures were those obtained from the second derivative of the original spectra. The areas of the bands were calculated by integration of the corresponding fitted band. A straight baseline passing through the ordinates at 1700 cm^{-1} and 1600 cm^{-1} was adjusted as an additional parameter to obtain a best fit. The curve-fitting procedure was performed by step-wise iterative adjustment towards a minimum root mean-square error of the different parameters determining the shape and position of the absorption peaks. It was carried out by assuming an initial mixed Lorentzian–Gaussian line-shape function, with full width band at half-height (FWHH) of $13\text{--}18\text{ cm}^{-1}$ and a maximum resolution factor. Baseline corrections, normalization, derivation, curve fitting and area calculation were carried out by means of Grams/32 (Galactic Industries Corporation, USA) software, OPUS 3.1 and Perkin-Elmer software. The resulting fitted curve was analyzed taking into account the band assignment for the secondary structure previously reported in the literature [29]: α -helix, $1658\text{--}1650\text{ cm}^{-1}$; β -sheets, $1637\text{--}1613\text{ cm}^{-1}$; turns, $1673\text{--}1666\text{ cm}^{-1}$; random coil, $1645\text{--}1637\text{ cm}^{-1}$; and β -antiparallel, $1695\text{--}1675\text{ cm}^{-1}$. In order to calculate the percentage contribution of the different types of conformations to the area of all the components, bands assigned to a given conformation were summed and divided by the total Amide I area.

2.5. Antioxidant properties

2.5.1. Superoxide dismutase assay (SOD)

The SOD mimetic activity was determined by a non-enzymatic method. In this method, the system (PMS, phenazine methosulfate)/ (NADH) produces the superoxide anion radical. The system contains 0.5 mL of sample, 0.5 mL of 1.404 mM NADH, and 0.5 mL of 300 μM NBT (nitroblue tetrazolium), in 0.05 M phosphate buffer (pH 7.5). After incubation at 25 °C for 15 min, the reaction starts by the addition of 0.5 mL of 120 μM PMS. The solutions of complex were prepared in hot dimethylsulfoxide (DMSO) before adding the phosphate buffer to obtain the desired final concentrations. The final DMSO to buffer concentration ratio never exceeded 5:100. Then, the reaction mixture was incubated for 5 min at 25 °C. For comparative purposes free ligand and free oxidovanadium(IV) were also tested under the same experimental conditions. The results were determined by reading the absorbance at 560 nm. The amount of compound that produced a 50% inhibition of NBT reduction was obtained from a plot of percentage of

inhibition versus compound concentration. Kinetic constant value (k), which is independent of both detector concentration and nature was calculated according to: $k_{MCF} = k_{\text{detector}} \cdot [\text{detector}] / IC_{50}(\text{compound})$, where k_{NBT} (pH = 7.8) = $5.94 \times 10^4 \text{ mol}^{-1} \text{ L s}^{-1}$, $[\text{detector}] = \text{detector concentration}$ [31].

2.5.2. 1,1-Diphenyl-2-picrylhydrazyl assay

A modified method of Yamaguchi et al. [20] was used in order to evaluate (triplicate measurements) the antiradical activity of chlorogenic acid and its complex. A methanolic solution of 1,1-diphenyl-2-picrylhydrazyl radical (DPPH) (4 mL, 40 ppm) was added to 1 mL of the antioxidant solutions in 0.1 M Tris–HCl buffer (pH 7.1) at 25 °C, giving final concentrations of 10, 25, 50, and 100 μM . After 60 min of the reaction in the dark, the absorbance at 517 nm was measured and compared with the absorbance of the control prepared in a similar way without the addition of the antioxidants (this value was assigned arbitrarily as 100%).

2.5.3. 2,2'-Azinobis (3-ethylbenzothiazoline-6-sulfonic acid) diammonium salt. Decoloration assay

The total antioxidant activity was measured using the Trolox (6-hydroxy-2,5,7,8-tetramethylchroman-2-carboxylic acid) equivalent antioxidant coefficient (TEAC). The radical cation of 2,2'-azinobis(3-ethylbenzothiazoline-6-sulfonic acid) diammonium salt (ABTS^{•+}) was generated by incubating ABTS with potassium persulfate. Chemical compounds that inhibit the potassium persulfate activity may reduce the production of ABTS^{•+}. This reduction results in a decrease of the total ABTS^{•+} concentration in the system and contributes to the total ABTS^{•+} scavenging capacity. Briefly, an aqueous solution of ABTS (0.25 mM) and potassium persulfate (0.04 mM) was incubated in the dark for 24 h. The solution was then diluted five times in 0.1 M KH_2PO_4 –NaOH buffer (pH 7.4). To 990 μL of this mixture, 10 μL of chlorogenic acid, the complex, or the Trolox standard in phosphate buffer was added (final concentrations 0–100 μM). The reduction of ABTS^{•+} was monitored spectrophotometrically 6 min after the initial mixing at 25 °C. The percentage decrease of the absorbance of the band at 734 nm was calculated considering that the basal condition (without antioxidant additions) had been assigned as 100% and was plotted as a function of the concentration of the samples giving the total antioxidant activity. The TEAC was calculated from the slope of the plot of the percentage inhibition of absorbance versus the concentration of the antioxidant divided by the slope of the plot for Trolox [20].

2.5.4. Scavenging of the hydroxyl radical

The ascorbate–iron– H_2O_2 system was used for hydroxyl radical's generation. In a few words, the reaction mixture contains 3.75 mM 2-deoxyribose, 2.0 mM H_2O_2 , 100 μM FeCl_3 , and 100 μM EDTA without or with the tested compounds in 20 mM KH_2PO_4 –KOH buffer, pH 7.4. The reaction was triggered by the addition of 100 μM ascorbate and the mixture was incubated at 37 °C for 30 min. Solutions of FeCl_3 , ascorbate, and H_2O_2 were made up in deaerated water immediately before use. Thiobarbituric acid method was applied to evaluate the extent of deoxyribose degradation by hydroxyl radical [20].

2.5.5. Inhibition of peroxy radical

Peroxy radicals were generated by the thermal decomposition of 2,2-azobis(2-amidinopropane) dihydrochloride (AAPH). AAPH was chosen due to its ability to generate free radicals at a steady rate for extended periods of time (half life of 175 h). The consumption of pyranine was followed spectrophotometrically by the decrease in absorbance at 454 nm with a thermostated cell at 37 °C. The reaction solutions contained AAPH (50 mM), pyranine (50 μM) and several concentrations of the tested compounds. The delay of pyranine consumption (lag phase) was calculated as the time before the consumption of pyranine started (notable reductions in absorbance) [20].

2.5.6. Cell culture

Human MDA-MD231, T47D, and SKBR3 breast cancer cell lines were obtained from HPA Culture Collection (Salisbury, United Kingdom). The first two cell lines were cultured in endotoxin-free RPMI medium supplemented with 10% FBS, 1% non-essential amino acids and 100 U/mL penicillin and 100 $\mu\text{g}/\text{mL}$ streptomycin. SKBR3 cells were cultured in endotoxin-free Mc Coy medium supplemented with 10% FBS and 100 U/mL penicillin and 100 $\mu\text{g}/\text{mL}$ streptomycin. All reagents were from Sigma–Aldrich (St. Louis, MO). Primary human mammary epithelial cells were obtained from ScienCell Research Laboratories and were grown in mammary epithelial medium supplemented with 1% mammary epithelial growth supplement and 100 U/mL penicillin and 100 $\mu\text{g}/\text{mL}$ streptomycin. Cultures were maintained at 37 °C in a humidified atmosphere with 5% CO_2 and passaged according to the manufacturer's instructions.

2.5.7. Cell proliferation and mechanism

Breast cancer cells MDAMB231, T47D, SKBR3 and primary human mammary epithelial cells were seeded at a density of 5000 cells/well in 96 well plates, grown overnight and treated with either vehicle, chlorogenic acid, VOchlorog and oxidovanadium(IV) of different concentrations in FBS free medium. The dissolution vehicle was DMSO to yield a maximum final concentration of 0.5% in the treated well (Sigma–Aldrich, St. Louis, MO). After 24 h of incubation, 3-(4,5-methylthiazol-2-yl)-2,5 diphenyl-tetrazolium bromide (MTT) was added at 100 $\mu\text{g}/\text{well}$ for 2 h (Sigma–Aldrich, St. Louis, MO).

The formazan products generated by cellular reduction of MTT were dissolved in DMSO and the optical density was measured at 450 nm using Sinergy 2 Multi Mode Microplate reader Biotek (Winooski, USA). All experiments were done in triplicate.

For the high content analysis image assay the MDAMB231, T47D and SKBR3 cells were seeded at a density of 5000 cells/well in a collagen-coated 96 well plate and stained with fluorescent probes (Invitrogen, Life Technologies, Madrid, Spain) during 30 min: tetramethyl rhodamine methyl ester (TMRM) 50 μM for the measurement of mitochondrial depolarization related to cytosolic Ca^{2+} transients, 5-(and-6)-chloromethyl-2,7-dichlorodihydrofluorescein diacetate acetyl ester (CMH2DCFDA) 1 μM for the determination of reactive oxygen species production (ROS) and CellEvent™ Caspase 3/7 Green Detection Reagent 5 μM for the assessment of caspase 3/7 activation. After 30 min cells were treated with 10 μM concentration of chlorogenic acid, VOchlorog and oxidovanadium(IV) during 24 h. Some cells received 100 μM H_2O_2 as positive control for ROS and TMRM measurement and 10 μM staurosporine as positive control for Caspase 3/7 activation. Image acquisition was performed using a Becton Dickinson Pathway plate imager with a 10 \times Olympus Objective. The excitation/emission filters for each probe were: 488/10 nm and 515 LP nm (ROS), 555/28 nm and 647/78 nm (TMRM), and 488/10 nm and 515 LP nm (CellEvent™ Caspase 3/7 Green Detection Reagent). Using specific AttoVision (BD) software algorithms, the mean intensity of each region of interest (ROI) was analyzed. After the measurements with the probes, conditioned medium from each well was collected for LDH assay. This assay was performed according to the manufacturer's protocol. LDH release to the culture medium was determined using a Sinergy 2 Multi Mode Microplate reader Biotek (Winooski, USA) at 340 nm. To detect DNA damage the cells were fixed with 3% paraformaldehyde for 30 min at room temperature and permeabilized with 0.3% triton for 10 min. Cells were blocked during 30 min with 3% BSA in PBS (phosphate-buffered saline). Then they were incubated with 2 $\mu\text{g}/\text{mL}$ mouse monoclonal H2AX (Abcam, Cambridge, United Kingdom) for 1 h at room temperature. The secondary antibody used was Alexa 633 goat anti-mouse. Images were acquired on a BD Pathway™ Bioimager (Becton Dickinson). At least three independent experiments were performed for each experimental condition in all the biological assays. The results are expressed as the mean \pm the standard error of the mean.

3. Results and discussion

3.1. Chemistry: characterization of the solid compound

3.1.1. Infrared spectroscopy

Tentative assignments (Table 1) were performed based on the data found in the literature [32–35].

Taking into account the available “donor groups” presented in chlorogenic acid, we would assume that metal interaction would occur via the carboxylate group. As it is expected, the formation of the sodium salt and the coordination of the metal through this group would lead to the splitting of the characteristic C=O stretching band of the carboxylic acid (ν_{CO}) of the free ligand to two new bands corresponding to antisymmetric and symmetric stretching modes of the new carboxylate group (COO^-). As can be seen in Table 1, in the sodium salt these bands appeared at 1597 cm^{-1} and 1383 cm^{-1} and in the complex at 1576 cm^{-1} and 1363 cm^{-1} , respectively. It is also well known that carboxylate group presents different ways of interacting (monodentate, bidentate, bridge, etc.) with metals. In order to analyze the possibility of any interaction with the cation oxidovanadium (IV), we proceed to the calculation of the difference $\Delta\nu = \nu_{\text{a}}(\text{COO}^-) - \nu_{\text{s}}(\text{COO}^-)$, which is used as a criteria to establish the coordination of the COO^- group to the metal. The value $\Delta\nu$ ($\nu(\text{COO}^-)_{\text{as}} - \nu(\text{COO}^-)_{\text{s}}$) calculated for the complex is 213 cm^{-1} similar to that obtained for the sodium salt (214 cm^{-1}) which suggests the presence of the carboxylate group in ionic form in the complex as in the sodium salt. Continuing our analysis, it can be seen that $\nu(\text{C}=\text{O})$ stretching band of the ester moiety remains unchanged after coordination, although its intensity decreases. This suggests that the C=O group probably is not involved in complex formation. Analyzing the vibrational modes related to the OH groups of the chlorogenic acid, it can be observed (Table 1) that the bands assigned to phenolate-stretching mode ($\nu(\text{CO})$) ($1273\text{--}1265\text{ cm}^{-1}$ region) shifted from their original position to 1278 cm^{-1} indicating the possibility of complexation with the oxidovanadium(IV) cation. Additional support for the proposed coordination mode was the location in

Table 1

Tentative assignments of some characteristic FTIR bands (cm^{-1}) of chlorogenic acid, chlorogenate sodium salt ($\text{Na}_3\text{chlorog}$) and $\text{Na}[\text{VO}(\text{chlorog})(\text{H}_2\text{O})_3]\cdot 4\text{H}_2\text{O}$ (VOchlorog).

Chlorogenic acid	$\text{Na}_3\text{chlorog}$	VOchlorog	Assignments
3364br			H bonds
3468h	3448br	3402br	$\nu(\text{OH})$ aryl [32]
2967m	2962w	2967w	$\nu(\text{C}=\text{C})$ ethylene
2924m	2924w	2924w	$\nu(\text{C}-\text{H})$ [32]
1717h			$\nu(\text{C}=\text{O})$ COOH
1689vs	1690s	1689s	$\nu(\text{C}=\text{O})$ [35]
	1597vs	1576h	$\nu(\text{COO}^-)_{\text{as}}$ [34]
1638m	1635vw	1624s	$\nu(\text{C}=\text{C})$ ethylene
1606m, 1522m,	1527s, 1465w	1522vw, 1484w,	$\nu(\text{C}=\text{C})$ aromatic ring
1445s		1433w	
1371h			$\nu(\text{C}=\text{C}) + \delta(\text{C}-\text{H})$
	1383s	1363m	$\nu(\text{COO}^-)_{\text{s}}$ [34]
1331h	1324m	1340h	$\beta(\text{C}-\text{H})\text{C}=\text{C} + \beta(\text{C}-\text{H}) +$
(C-O) phenol			
1287s	1287h		$\nu(\text{C}-\text{OH}) + \delta(\text{C}-\text{OH})$
	1273s	1265vs	$\nu(\text{C}-\text{O})$ phenol
1191s	1177vs	1180h	$\delta(\text{C}-\text{OH}) + \beta(\text{C}-\text{H})$ [33]
	1145vw	1156m	$\delta(\text{C}-\text{OH}) + \beta(\text{C}-\text{H})$
1120w, 1081w,	1119m, 1081m,	1117w, 1086h,	$\beta(\text{C}-\text{H})$
1039w	1034m	1037vw	
973m	969m	976m	$\gamma(\text{C}-\text{H})\text{C}=\text{C} + \gamma(\text{C}-\text{H})$
		945s	$\nu(\text{V}=\text{O})$ [33,36]
907w	925w	921h	$\delta(\text{C}-\text{OH})$
852vw	843w	871h	$\gamma(\text{C}-\text{H})$ [32]
816m	811m	818m	$\beta(\text{C}=\text{O})$
740vw	720vw	760vw	$\nu(\text{CC}) + \delta(\text{CCC})$ [32]
		666vw	$\nu(\text{V}-\text{O})$ phenol

Relative intensities of the bands: vs: very strong, s: strong, m: medium, w: weak, vw: very weak, h: shoulder, br: broad, β , in-plane bending mode, α , binding mode in the flat aromatic ring; γ , out of plane bending mode.

the spectrum of the band associated with the $\nu(\text{V}=\text{O})$ stretching mode that appeared at 945 cm^{-1} . Usually, when the metal interacted with the carboxylate moiety this band is found around $990\text{--}980\text{ cm}^{-1}$. The shift towards lower frequencies could be produced after the coordination with the deprotonated OH groups of the ligand that will cause the weakening of the V=O bond. This behavior can be observed for sigma donor ligands (glucuronic acid, nonsteroidal antiinflammatory drugs, etc.) in which this band is located around $930\text{--}940\text{ cm}^{-1}$ suggesting that the coordination occurs through deprotonated cis-OH groups of the molecules [36]. The spectrum also shows the presence of a band at 666 cm^{-1} assigned to the V–O phenolic stretching and the displacement of the band assigned to the $\nu(\text{OH})$ aryl mode to lower frequencies supporting together the postulated mode of coordination.

3.1.2. EPR spectroscopy

In order to establish the coordination sphere around oxidovanadium(IV) ion in the solid complex, X-band-EPR spectrum was measured at room temperature. The spectrum shows the typical eight-line hyperfine splitting patterns due to the unpaired electron of the ^{51}V nucleus ($I = 7/2$), demonstrating the presence of one mononuclear oxidovanadium(IV) species in $\text{Na}[\text{VO}(\text{chlorog})(\text{H}_2\text{O})_3]\cdot 4\text{H}_2\text{O}$ compound (Fig. 2A). The experimental spectrum had been simulated based on the calculated EPR parameters and the fitting was in agreement with the experimental one (Fig. 2B). The simulation predicted that the new observed signal was originated by a V-chromophore being consistent with the oxidovanadium(IV) ion in a nearly axial or pseudoaxial ligand field. The spin Hamiltonian parameters were $g_{\parallel} = 1943$ and $g_{\perp} = 1981$ and the hyperfine coupling constants, $A_{\parallel} = 170 \times 10^{-4}\text{ cm}^{-1}$ and $A_{\perp} = 61 \times 10^{-4}\text{ cm}^{-1}$ ($g_{\text{iso}} = 1.968$, $A_{\text{iso}} = 97.33 \times 10^{-4}\text{ cm}^{-1}$). The parallel component of the hyperfine coupling constant is sensitive to the donor atoms on the equatorial coordination sphere of the metal center. By using the well known “additivity relationship” introduced by Chasteen [20–22], the identity of the equatorial ligands in $\text{V}(\text{IV})\text{O}^{+2}$ complexes can be determined as: $A_{\parallel} = \sum n_i A_{z,i}$ (n_i : number of equatorial ligands of type I, $A_{z,i}$: contribution to the parallel hyperfine coupling from each of them). Taking into account the elemental analysis and the FTIR results it was assumed that two Ar–O $^-$ groups ($A_{\parallel} = 2 \times 38.6 \times 10^{-4}\text{ cm}^{-1}$) and two water molecules ($A_{\parallel} = 2 \times 45.7 \times 10^{-4}\text{ cm}^{-1}$) [19] are coordinated to the metal in the equatorial plane giving an estimated final A_{\parallel} value of $168.6 \times 10^{-4}\text{ cm}^{-1}$ which agrees reasonably well with the experimental value from the simulation.

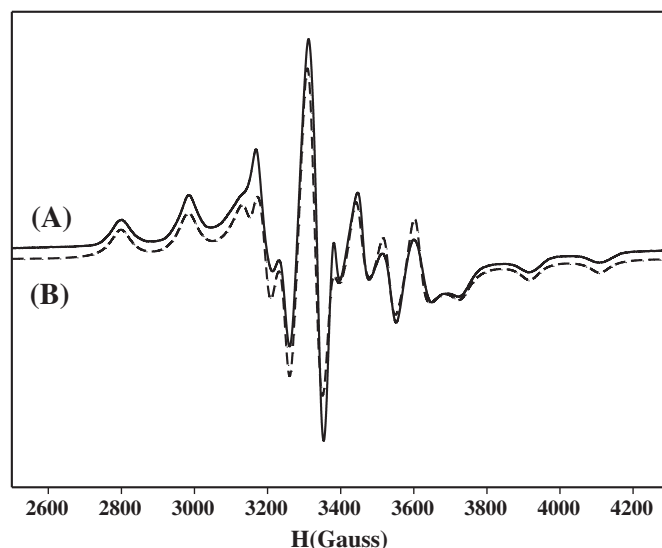


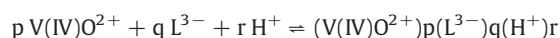
Fig. 2. Experimental (A) and calculated (B) powder EPR spectra of VOchlorog measured at X-band (9.4006 GHz, 290 K).

Considering that the analytical data and the TGA measurements confirm the composition of the solid complex and the proposed stoichiometry, taking into account the evidences of the coordination mode of the ligands obtained by the FTIR spectra and bearing in mind the geometry assumed from the diffuse reflectance spectra and EPR spectroscopies, it is then possible to presume that in the equatorial position around the oxidovanadium(IV) cation, there are two Aryl-O⁻ groups from the ligand and two water molecules and with the axial position being occupied by the third water (Fig. 3).

4. Solution speciation profiles: stability constants and electron paramagnetic resonance measurements

The speciation model for the L³⁻/V(IV)O²⁺/H⁺ (L: chlorogenate anion) system and the corresponding formation constants for the species are shown in Table 2.

The formation constants of the species (β pqr) are expressed using the notation:



A value of $\text{pK}_w = 13.76$ (corresponding to $\log \beta_{0-1} = -13.76$) was assumed for the experimental conditions ($T = 25^\circ\text{C}$, $I = 150 \text{ mM}$).

During the formulation of the speciation analysis various species were tested in the system including mono and bimetallic complexes but they should be discarded to achieve the best fit with the experimental data. Although the aqueous equilibrium of the ligand has been extensively studied, deprotonation constants were recalculated from different sets of titrations using Best calculation program [37]. The calculated data of the chlorogenic acid (H₃L), $\text{pK}_1 = 3.42$, $\text{pK}_2 = 8.35$ and $\text{pK}_3 = 12.25$ were comparable with those reported in the literature [38]. In relation to the pK_3 value appreciable dispersion in the reported values can be observed, probably attributed to the limitations of the glass electrode at high pH values. Hydroxo complexes of oxidovanadium(IV) were taken into account and the following species were assumed $[\text{VO}(\text{OH})_3]^+$ ($(\text{VO})\text{H}_{-1}^+$), $\log \beta = -5.50$, $[\text{VO}(\text{OH})_3]^-$ ($(\text{VO})\text{H}_{-3}^-$), $\log \beta = -17.90$ and $[\text{VO}_2(\text{OH})_5]^-$ ($(\text{VO})_2\text{H}_{-5}^-$), $\log \beta = -21.85$.

In order to determine the formation constants of the L³⁻/V(IV)O²⁺/H⁺ (L: chlorogenate anion) system, data collected from several sets of titrations were analyzed with Best and Superquad calculation programs [37]. Data were collected from acidic conditions up to pH approximately 11. The usual criteria for this kind of programs

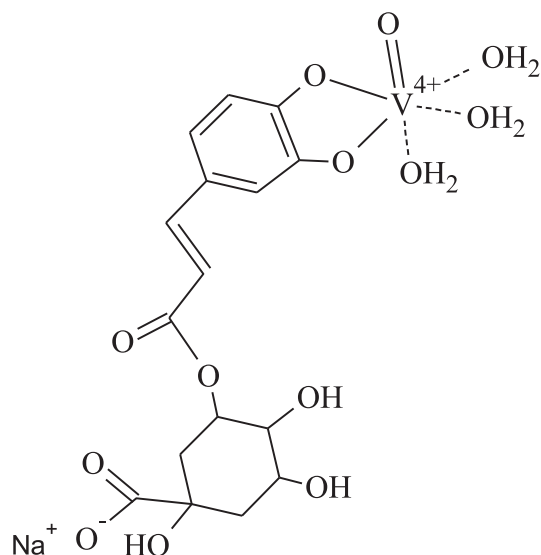


Fig. 3. Proposed coordination binding mode in VOchlorog complex.

Table 2

Composition, notation and formation constants (β) for L³⁻/V(IV)O²⁺/H⁺ system. Total concentration: V(IV)O²⁺: 2.5 mM, H₃L: 5.0 mM (0.150 M NaCl, 25 °C). H₃L: = chlorogenic acid, L: chlorogenate anion.

Species (pqrs)	Formula	log β
011	HL ²⁻	12.25
012	H ₂ L ⁻	20.60
013	H ₃ L	24.02
110	[VOL] ⁻	16.44
122	[VO(HL) ₂] ²⁻	40.88
120	[VOL ₂] ⁴⁻	31.11
10-1	[VOH ₋₁] ⁺	-5.50
10-3	[VOH ₋₃] ⁻	-17.90

(CHI², R values, standard deviations, etc.) were used to select the speciation model.

The species distribution diagram as a function of pH was obtained using SPECIES program. Fig. 4 shows the diagram, calculated for the total concentrations of: L: 5.0 mM and V(IV)O²⁺: 2.5 mM in the 2–7.5 pH-range. As shown in the diagram, free aqueous oxidovanadium(IV) ([VO(H₂O)₅]²⁺ (V(IV)O²⁺)) occurs at low pH values. As the pH increases (2.5–6) two species coexist, VO(LH)₂²⁻ and VOL⁻, and when the pH is above 6, the species VOL₂⁴⁻ becomes predominant. It is noteworthy that the model predicts for a concentration ratio of L:V(IV)O²⁺ 1:1 with the presence of the VOL⁻ as the major solution species in a pH range between 4.2 and 6.20 (data not shown). This prediction of pH and stoichiometry of the reactants were taken into account for the synthesis of the solid complex.

EPR spectra of the aqueous solution at 120 K were recorded at different pH values in order to assist in the identification of different oxidovanadium(IV) species and the corresponding geometries, particularly, the equatorial donor set. The variation of the EPR spectra with the pH is shown in Fig. 5. Table 3 shows the EPR parameters. The changes observed in the EPR spectra agree with the proposal of the speciation model. At pH = 2 (Fig. 5), the EPR signal shows the characteristic line-wide trends for free [VO(H₂O)₅]²⁺ ion (V(IV)O²⁺) denoting that no interaction occurs in high acidic medium. By adding NaOH 1 M aqueous solution, the increase of the pH value to 2.8 induces important variations on EPR features and one new resonance line appears together with the signal belonging to free vanadyl aquoion. The simulation predicts that the new observed signal (Fig. 5, [VO(LH)₂]²⁻) is originated by a V-chromophore with the spin Hamiltonian parameters of $g_z = 1.940$, $g_y = 1.977$, and $g_x = 1.987$ and the hyperfine coupling constants of $A_z = 175.10^{-4} \text{ cm}^{-1}$, $A_x = 69.10^{-4} \text{ cm}^{-1}$ and $A_y = 69.10^{-4} \text{ cm}^{-1}$ ($g_{\text{iso}} = 1.968$, $A_{\text{iso}} = 104.3.10^{-4} \text{ cm}^{-1}$). According to the speciation

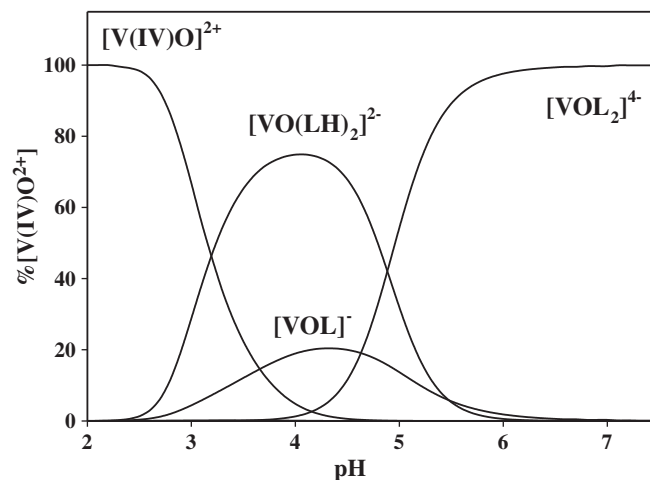


Fig. 4. Species distribution for the L³⁻/V(IV)O²⁺/H⁺ (L: chlorogenate anion) system as a function of pH. Total concentration V(IV)O²⁺: 2.5 mM, L: 5.0 mM, 25 °C, I = 0.150 M NaCl.

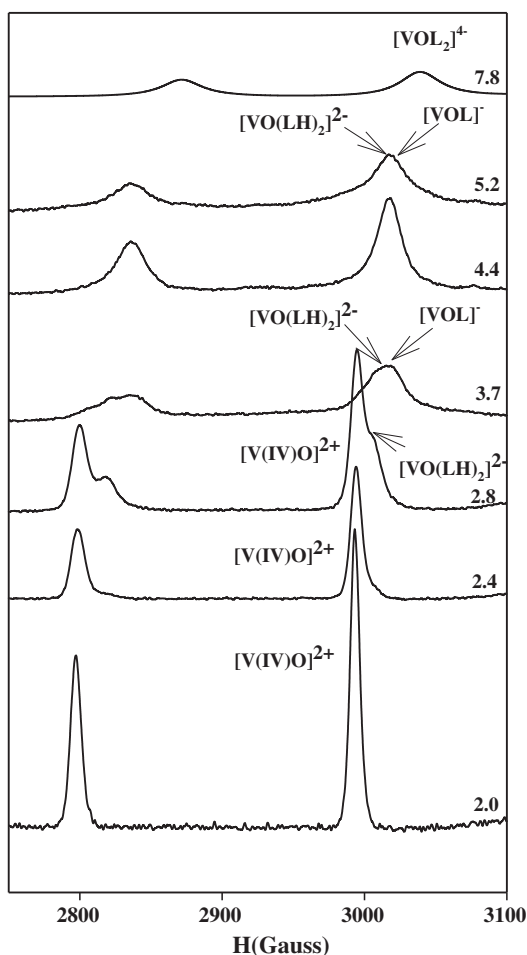


Fig. 5. X-band EPR spectra (A region) of the $L^{3-}/V(IV)O^{2+}/H^+$ (L: chlorogenic acid) system (frozen solutions, 140 K) in ratio $R = 2$, (A) as a function of pH. Total concentration $V(IV)O^{2+}$: 2.5 mM, L: 5.0 mM, 25 °C, $I = 0.150$ M NaCl.

diagram (Fig. 4) at pH 3.7, the presence of two species complex called $[VO(LH)_2]^{2-}$ and $[VOL]^-$ is predicted. In concordance, a new signal ($[VOL]^-$) in the EPR spectrum recorded at pH 3.7 (Fig. 4B) that overlapped with the signal of $[VO(LH)_2]^{2-}$ is observed.

For the new signal ($[VOL]^-$) the calculated EPR parameters are $g_z = 1.944$, $g_x = 1.975$, and $g_y = 1.982$ and the hyperfine coupling constants of $A_z = 169.10 \cdot 10^{-4} \text{ cm}^{-1}$, $A_x = 56.10 \cdot 10^{-4} \text{ cm}^{-1}$ and $A_y = 62.10 \cdot 10^{-4} \text{ cm}^{-1}$ ($g_{iso} = 1.967$, $A_{iso} = 95.66 \cdot 10^{-4} \text{ cm}^{-1}$) suggesting the formation of a new complex with some modifications of the equatorial coordinated groups. At pH above 5 the speciation diagram predicts the presence of a single species named $[VOL_2]^{4-}$ in coincidence with single signal registered at pH 7.8 in the EPR spectrum and the disappearance of the species $[VO(LH)_2]^{2-}$ and $[VOL]^-$. For the species $[VOL_2]^{4-}$, the calculated EPR parameters are: $g_z = 1.955$, $g_x = 1.978$, and $g_y = 1.982$ and $A_z = 155.10 \cdot 10^{-4} \text{ cm}^{-1}$, $A_x = 50.10 \cdot 10^{-4} \text{ cm}^{-1}$ and $A_y = 52.10 \cdot 10^{-4} \text{ cm}^{-1}$ ($g_{iso} = 1.972$, $A_{iso} = 85.67 \cdot 10^{-4} \text{ cm}^{-1}$) in

correspondence with a new modification of the coordination sphere around the metal center.

By using the “additivity rule” and considering the contributions to the parallel hyperfine coupling constant of the different coordination modes of the ligand and the solvent ($COO^- = 42.1$, $ArO^- = 38.6$ and $H_2O = 45.7 \times 10^{-4} \text{ cm}^{-1}$ [19,21,40], respectively) the empirical $A_{||}$ was estimated for all the detected species. Free $[VO(H_2O)_5]^{2+}$ (Fig. 5, $V(IV)O^{2+}$) can be identified with a $A_{||} = 182.8 \times 10^{-4} \text{ cm}^{-1}$.

Regarding the potential coordination sites available in chlorogenic acid, it should be noted that there is one carboxylate group (o carboxylic acid group) belonging to the quinic acid moiety of the molecule and OH residues present in the phenolic rings. The interaction observed at low pH values with the occurrence of the species $[VO(LH)_2]^{2-}$ makes it possible to deduce the presence of the carboxylate moiety in the coordination sphere. Assuming that the speciation diagram shows the presence of doubly deprotonated ligand coordinated to the metal and considering the pKa value of 3.42 for chlorogenic acid ($-COOH$ group), it can be speculated that only the carboxylate group may eventually interact with the metal center. On this basis, suggesting an equatorial coordination sphere with two carboxylate groups from two ligands and two water molecules, the calculation of $A_{||}$ indicates a value of $175.6 \times 10^{-4} \text{ cm}^{-1}$ ($A_{||} H_2O = 45.7 \times 10^{-4} \text{ cm}^{-1}$, $A_{||} -COO^- = 42.1 \times 10^{-4} \text{ cm}^{-1}$) in excellent correlation with the value obtained by simulation of the spectrum. The probable interaction of metal through deprotonated phenolic O^- group is discarded based on the calculated value for the hyperfine coupling constant and the high concentration of protons in the solution.

Previous existing studies about the interaction of this ligand with different metals [32–35] predict that with increasing the pH value of the medium, subsequent points of interaction are possible via deprotonation and coordination through OH residues from the phenolic rings of the molecule. This is essentially due to changes occurring in the electronic distribution in the phenyl ring and the carbonated chain and, in effect, the ring acquires a quinoidal conformation decreasing the CC bond lengths and in consequence is accompanied by an alteration in the electron distribution of the substituents for preserving conjugation. Thus, ruling out the possibility of an interaction via the aliphatic hydroxyl group located at the adjacent position of the carboxylate group, the coordination probably takes place through the deprotonated OH^- groups in the aromatic ring of the molecule [37]. Considering this previous information, and being in concordance with those predicted by the species distribution diagram, for the species $[VOL]^-$ the ligand could coordinate through the two ArO^- groups in cis-position of only one ligand and two water molecules in the equatorial plane. This assumption leads to a calculation of $A_{||} = 169.2 \times 10^{-4} \text{ cm}^{-1}$ ($A_{||} H_2O = 45.7 \times 10^{-4} \text{ cm}^{-1}$, $A_{||} ArO^- = 38.9 \times 10^{-4} \text{ cm}^{-1}$) with this value being in good correlation with the experimental one (Table 3). At higher pH values, a new EPR signal was detected. From the simulation of their EPR parameters it is possible to observe the reduction of A_z ($A_{z \text{ calc}} = 155 \times 10^{-4} \text{ cm}^{-1}$). This trend is attributed to changes in the coordination sphere of the vanadyl moiety, probably including additional coordination of the alkoxide group of the ligand and/or incorporation of another O^- group to the coordination sphere. We can assume for the species called $[VOL_2]^{4-}$ a coordination in the equatorial plane that includes four ArO^- groups from two ligands interacting with the oxidovanadium(IV) cation. If we

Table 3
EPR parameters for the for $L^{3-}/V(IV)O^{2+}/H^+$ (L: chlorogenate anion; 5 mM: 2.5 mM) system.

Species	Equatorial coordination set	$g(x)$	$g(y)$	$g(z)$ or $g_{ }$	g_{iso}	$A(x)^a$	$A(y)^a$	$A(z)$ or $A_{ }^a$	A_{iso}
$[V(IV)O]^{2+}$	$4H_2O$	1.982	1.977	1.935	1.965	70	70	182	107.3
$[VO(LH)_2]^{2-}$	$2COO^-, 2H_2O$	1.987	1.977	1.940	1.968	69	69	175	104.3
$[VOL]^-$	$2ArO^-, 2H_2O$	1.975	1.982	1.944	1.967	56	62	169	95.66
$[VOL_2]^{4-}$	$4ArO^-$	1.978	1.982	1.955	1.972	50	52	155	85.67

^a A values in 10^{-4} cm^{-1} .

make the prediction of the value of A_{11} ($A_{11} \text{ArO}^- = 38.6 \times 10^{-4} \text{ cm}^{-1}$) it shows a value of $154.4 \times 10^{-4} \text{ cm}^{-1}$ which agrees well with the simulated EPR spectrum obtained in this pH range. As it is expected, species containing O^- groups around the oxidovanadium(IV) cation were usually identified as proposed in speciation studies [39]. The calculated A_z value matched well with other possibilities ($A_z (2\text{ArO}^- + 2\text{OH}^-) = 154.6$ and $A_z (1\text{ArO}^- + 3\text{OH}^-) = 154.7$) or $\text{VO}(\text{OH})_3(\text{H}_2\text{O})_2^-$ and $\text{VO}(\text{H}_2\text{O})_5(\text{OH})$ [40] which were consistent with the hypothesis of the presence of the hydrolytic complex. However these ligand-containing species were systematically discarded during the calculations. The formation of the ligand-free hydrolytic species could not be accurately established. They are not significantly predicted by the species diagram perhaps because their occurrence in very low concentration makes it difficult to detect in our experimental conditions.

If we formulate an analysis of the founded 1:1 M:L species in comparison with previous studies with other metal cations (Pb(II) [41], Al(III) [42], Fe(II) and Cu(II) [43]), it can be observed that there is a clear tendency in the alkaline pH range (4.0–6.5) to form a solution complex with 1:1 M:L relationship. Formation of bimetallic species only has been proposed for Cu(II) and Pb(II) [41]. These findings allowed us to choose the adequate experimental conditions to isolate the solid complex. The presence of non-oxo vanadium(IV) species, given the violet color of the complex, has been ruled out by EPR spectroscopic measurements.

5. Antioxidant properties

Since chlorogenic acid, which is one of non-flavonoid phenolic compounds present in the diet, acts as antioxidant agent, the antioxidant properties of the $\text{V}(\text{IV})\text{O}^{2+}$ species, chlorogenic acid and VOchlorog were studied. Concerning the ability to scavenge the radical DPPH^\bullet , the system with chlorogenic acid was consistent with the findings in the literature. When $50 \mu\text{M}$ of chlorogenic acid was tested, 84% of the inhibition of the DPPH^\bullet radical was observed (Fig. 6A). When a concentration of $100 \mu\text{M}$ was used, the ligand inhibited 85% of DPPH^\bullet radical while the complex acts as a better antioxidant agent exerting 93% of inhibition on DPPH^\bullet radical at the same concentration. Based on these results it can be assumed that complexation improves the antioxidant effect.

The hydrogen-donating ability of $\text{V}(\text{IV})\text{O}^{2+}$ species, chlorogenic acid and VOchlorog by evaluating $\text{ABTS}^{\bullet+}$ scavenging is presented in Fig. 6B. It can be seen that at higher concentrations of chlorogenic acid and its complex with oxidovanadium(IV) (50 and $100 \mu\text{M}$) both behave like Trolox, sequestering almost 95% of radical cation $\text{ABTS}^{\bullet+}$. At lower concentrations (10 and $25 \mu\text{M}$) the ligand acts more efficiently than VOchlorog. The activity is expressed as the millimolar concentration of Trolox (TEAC) equivalent to the activity of a 1 mM solution of the experimental compound. The TEAC value of 1.18 calculated for the chlorogenic acid agrees with the reported data (TEAC: 0.98 and 1.30 [44]) while the value of 1.66 obtained for VOchlorog demonstrates that both are in the same order of magnitude. Therefore for this experiment complexation does not enhance the free ligand activity.

In relation with the SOD mimic activity of the ligand, literature data based in different methodologies give values of IC_{50} of $41.0 \pm 12 \mu\text{M}$ according to the MPEC method (2-methyl-6-metoxifenilnitimidazopirazinona) [8], a concentration of $\text{O}_2^{\bullet-}$ radical of 31.3 ± 3.3 to $50 \mu\text{M}$ by using electron paramagnetic resonance measurements [45] and 80% of sequestrant power of anion radical at $100 \mu\text{M}$ concentration when the radical anion is generated through the xanthine–xanthine oxidase system [46]. Our measurements (Fig. 7A) led to an IC_{50} value of $1035 \mu\text{M}$ for chlorogenic acid and $20.46 \mu\text{M}$ for the VOchlorog complex. It should be noted that reported IC_{50} values are dependent both on the detector used (usually cytochrome c Fe(III) or nitroblue tetrazolium (NBT)) and on its concentration. So, IC_{50} values are not appropriate for comparisons with the literature data. For that reason the kinetic constant value (k_{MCCF}), which is independent of both detector concentration and

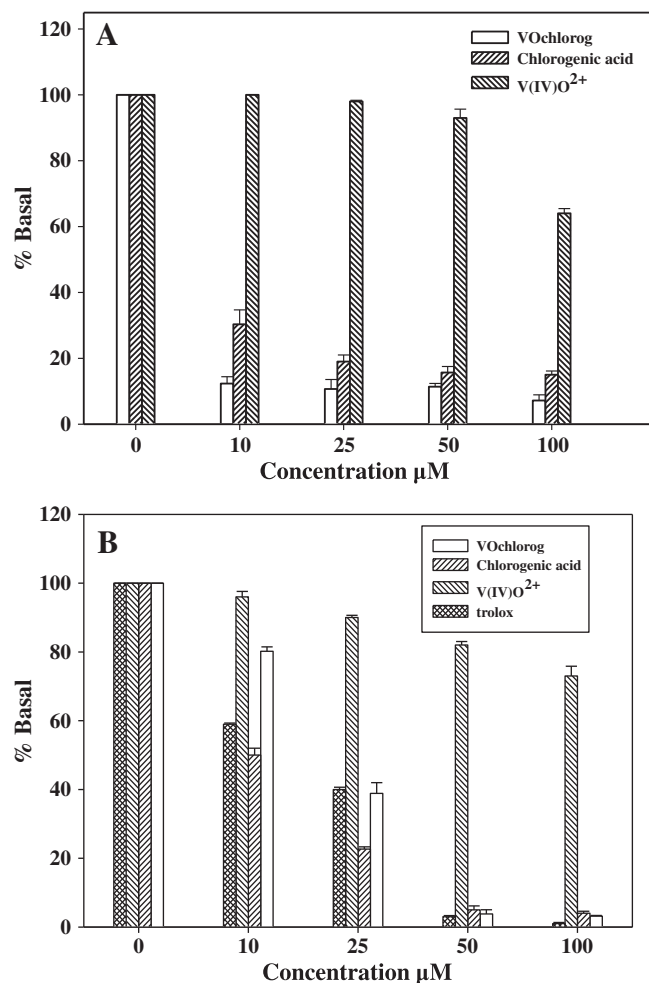


Fig. 6. (A) Effects of $\text{V}(\text{IV})\text{O}^{2+}$, chlorogenic acid and VOchlorog on the reduction in the concentration of DPPH^\bullet radical. (B) Total antioxidant activity measured as the reduction of the concentration of $\text{ABTS}^{\bullet+}$ caused by the addition of $\text{V}(\text{IV})\text{O}^{2+}$, chlorogenic acid, VOchlorog and Trolox. Values are expressed as the mean \pm SEM of at least three independent experiments.

nature was calculated k_{MCCF} for chlorogenic acid giving a value of $1.7 \times 10^4 \text{ M}^{-1} \text{ s}^{-1}$ close with the literature value of $1.5 \times 10^4 \text{ M}^{-1} \text{ s}^{-1}$ [7]. The calculated value for the complex $k_{\text{MCCF}} = 8.7 \times 10^5 \text{ M}^{-1} \text{ s}^{-1}$ strongly indicated an improvement of the catalytic activity under complexation. This strong enhancement of the antioxidant ability after complex formation is also demonstrated when the scavenging hydroxyl radical capacity was measured by the reduction of chromogen formation. As can be observed from Fig. 7B, when the concentration is $100 \mu\text{M}$, the complex suppressed 70% of the basal (the radical activity) but the ligand only suppressed 30% of the activity, clearly demonstrating that the complexation enhances the scavenger activity on OH^\bullet radical. It is worth mentioning that there are some discrepancies in the literature data for the scavenging capacity on hydroxyl radical for chlorogenic acid, with the reported results being quite different from each other [47,48]. In this work we compared both ligand and complex by using the same assay and the same experimental conditions.

Finally, the ORAC assay was performed. The inhibition peroxy radical assay is based on the ability of antioxidants to sequester the peroxy radical (ROO^\bullet). Typical pyranine decay curves are presented in Fig. 8(A, B), which shows the effect of chlorogenic acid (left) and its complex with oxidovanadium(IV) (right) on pyranine consumption by radical ROO^\bullet . It is possible to conclude that for all tested concentrations, VOchlorog is a better peroxide scavenger agent than chlorogenic acid. The slopes of the curves of induction time versus concentration (Fig. 8, C and D)

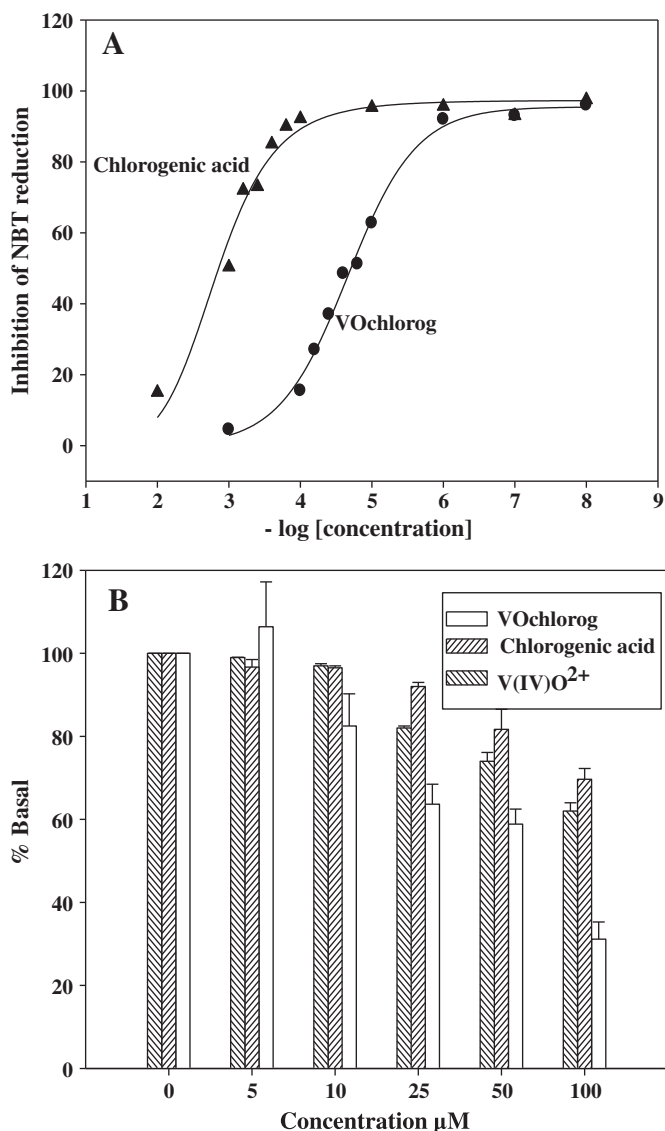


Fig. 7. (A) Effects of chlorogenic acid and VOchlorog on the reduction of nitroblue tetrazolium by nonenzymatically generated superoxide (phenazine methosulfate and reduced nicotinamide adenine dinucleotide system). (B) Effect of V(IV)O²⁺, chlorogenic acid and VOchlorog on the extent of deoxyribose degradation by hydroxyl radical, measured with the thiobarbituric acid method. The values are expressed as the mean \pm SEM of at least three independent experiments.

indicated a higher reactivity of VOchlorog with AAPH-derived peroxy radicals, inhibiting the free radical damage to pyranine, and a lower reactivity of chlorogenic acid towards the peroxy radicals enhancing the pyranine oxidation (experimental slopes: 0.358, 0.886, and 5.24 for Trolox, chlorogenic acid and VOchlorog, respectively). Moreover, at 10 μ M this effect may be evidenced by an increase of lag phase (35.0 min) in the complex in comparison with the free ligand (5.8 min). In general our experiments showed that complex formation improved antioxidant activity manifested by the ligand. It can be concluded that VOchlorog behaves as good antioxidant agent with strongest inhibitory effects on O₂⁻, OH[•] and ROO[•] radicals.

6. Anticancer activity

6.1. Human breast cells. Cell viability assay (MTT method)

Breast cancer is the most frequently diagnosed cancer and the leading cause of cancer death among females, accounting for 23% of the total

cancer cases and 14% of the cancer deaths [49]. With the exception of a few anticancer agents, most breast cancer chemotherapeutics currently used have devastating effects on normal cells. So, the research is focused in finding compounds that act selectively on the cancer cells with slight toxicity in the normal breast cells.

The effects at 10 μ M concentration of chlorogenic acid, VOchlorog and the oxidovanadium(IV) cation on three breast cancer cells (SKBR3, T47D and MDAMB231) and primary human mammary epithelial viability are shown in Table 4. It can be seen that both chlorogenic acid and its oxidovanadium(IV) complex were not cytotoxic against MDAMB231 and T47D cancer cells. On the other hand, the effect of the free ligand on the SKBR3 cancer cell viability was not significant and the complex behaved as a more deleterious agent (inhibiting cell viability 40% at 10 μ M). These results indicate that the complexation improved the action of the ligand in these lines. The breast epithelial mammal cells were selected as the normal cell line and are not affected by the addition of 10 μ M of chlorogenic acid or oxidovanadium(IV) cation but VOchlorog was slightly cytotoxic (inhibiting cell viability 16% at 10 μ M).

The effectiveness of the cytotoxic effect against human cancer cells of the oxidovanadium(IV) complex in comparison with other metal complexes, can only be performed in cases in which the same experimental assay was applied or under the same experimental conditions (in vitro evaluation of the complexes, using the MTT methodology). We found that the effects of METVAN [27] and Ru(II) [50] and Pd(II) [51] on MDA-MB-231 viability were investigated. All of them seem to be more effective than VOchlorog complex with their IC₅₀ values being 0.5 μ M for METVAN, a range of 5.4–15.7 μ M for Ru(II) complexes and a range of 8.0–35 μ M for Pd(II) complexes. One example in which the activity on this cell line is similar to VOchlorog was in the complex of Pd(II) with 3-*O*-Benzyl-5-deoxy-1,2-*O*-isopropylidene-5-(4-(2-pyridyl)-1H-1,2,3-triazol-1-yl)- α -D-xylofuranose. For T47D cell line there were almost three Ir(III) complexes tested, but the cell proliferation was assessed by the crystal violet bioassay [52]. Against SKBR3 cancer cell line *cis*-(dichloro)tetraammineruthenium(III) chloride has been reported with selective cytotoxicity [53]. To our knowledge, this is one of the few reports of oxidovanadium(IV) complex with potent activity against SKBR3 cancer cell line. Thus, we can suggest that VOchlorog complex exhibited selective activity against this type of cancer cell line and the following studies were performed in order to elucidate the potential mechanisms of action.

6.2. Mechanisms of the effect of chlorogenic acid and VOchlorog in the T47D, MDAMB231 and SKBR3 cell lines

There are several reported cellular mechanisms related to the anticancer effects of vanadium compounds [19]. These effects appear to be exerted mainly through cell cycle arrest. Some of them emerged from the inhibition of protein phosphotyrosines (PTPs), others through activation of mitogen activated protein kinase (MAPK superfamily) signaling pathway or by interaction with deoxyribonucleic acid (DNA). There are also other signaling pathways activated by vanadium which may lead to apoptosis: production of reactive oxygen species in the cytosol or in the mitochondria resulting in mitochondrial damage and cytochrome C release which activates the caspases [19].

Based on the previous considerations, with the aim to confirm the possible cell death pathway we have investigated the effects of compounds on intracellular ROS production, mitochondrial membrane potential disruption, caspase 3/7 activation, nuclear damage and LDH release. The mechanism of action was studied in the tumoral cell lines, working at 10 μ M concentrations and with 24 h of incubation in order to obtain a reasonable number of viable cells. In agreement with the effects observed in the viability assays, the parameters studied were not affected after the treatment with 10 μ M solutions of the free ligand and its oxidovanadium(IV) complex in MDAMB231 and T47D cell lines (Table 5).

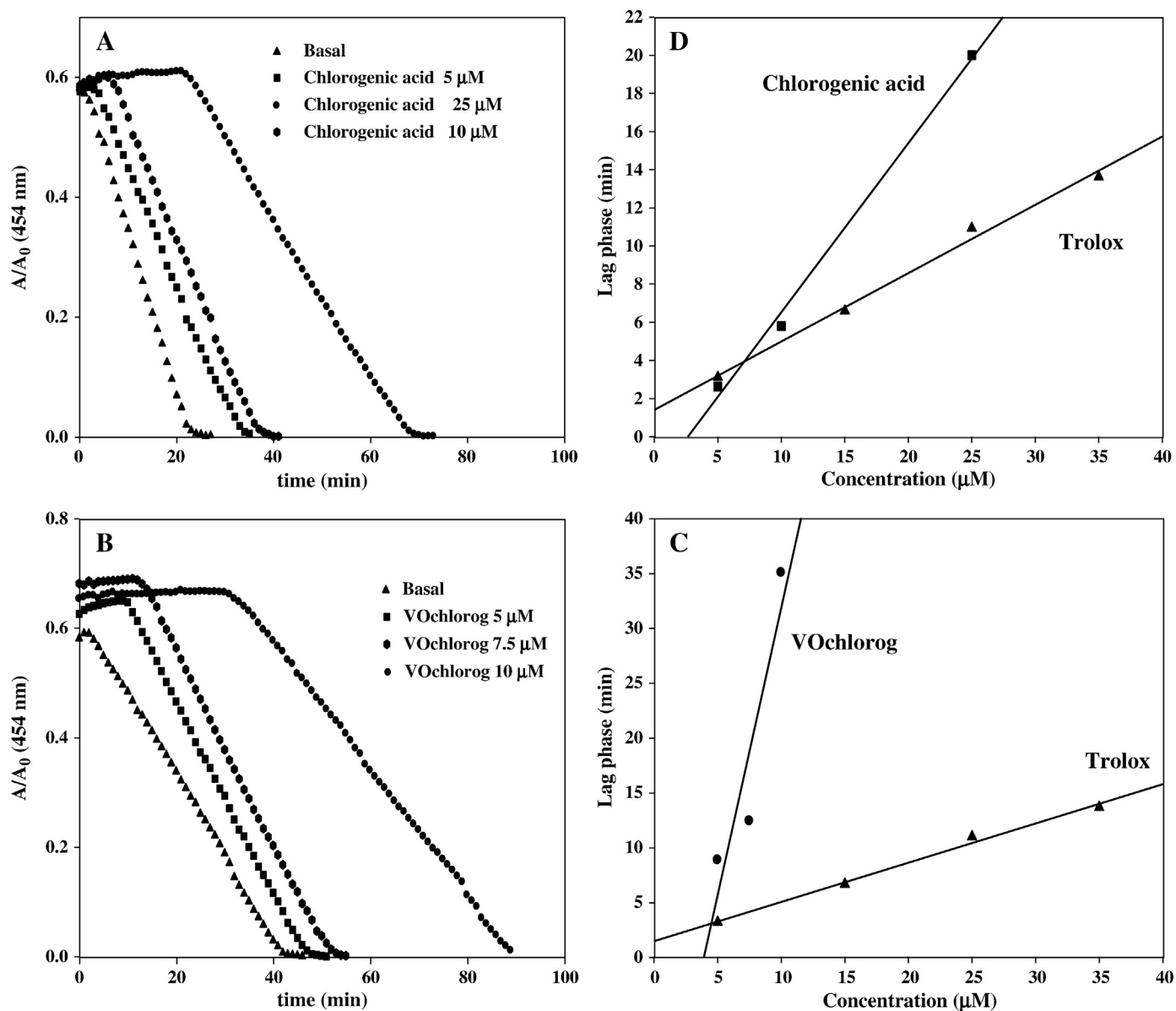


Fig. 8. Scavenging of peroxy radicals measured as the decay of the intensity of pyranine by addition of different concentrations of chlorogenic acid (A) and VOchlorog (B) (A_0 , initial intensity, 454 nm). Effect of chlorogenic acid and Trolox (C); and VOchlorog and Trolox (D) on AAPH-generated peroxy radicals and pyranine mixture. Changes on time delay (lag phase) upon the different concentrations of added substances.

To corroborate the possible role of oxidative stress in the VOchlorog-induced cytotoxicity in the SKBR3 cell line, the cells were incubated with CM-H2DCFDA probe. Results showed that compound did not

Table 4

Effects of chlorogenic acid, VOchlorog and $V(IV)O^{2+}$ on human breast cells. T47D and MDAMB231 cells were cultured in endotoxin-free RPMI medium supplemented with 10% FBS, 1% non-essential amino acids and 100 U/mL penicillin and 100 μ g/mL streptomycin.

	Percent survival		
	Chlorogenic acid	VOchlorog	$V(IV)O^{2+}$
SKBR3	90.1 \pm 2.4	60.7 \pm 7.4	77.6 \pm 2.0
T47D	116.6 \pm 12.0	110.8 \pm 7.0	92.5 \pm 1.6
MDAMB231	95 \pm 1.4	95 \pm 1.6	72.9 \pm 2.9
Breast epithelial cells	124.3 \pm 8.6	84.2 \pm 3.1	119 \pm 6.5

SKBR3 cells were cultured in endotoxin-free Mc Coy medium supplemented with 10% FBS, 100 U/mL penicillin and 100 μ g/mL streptomycin. Human breast epithelial cells were grown in mammary epithelial medium. Cells were incubated alone (basal) or with 10 μ M of the compounds at 37 $^{\circ}$ C for 24 h. The results are expressed as the percentage of the basal level and represent the mean \pm SEM.

increase the ROS production. This behavior could be explained by the fact that the oxidovanadium(IV) complex is a very important superoxide and peroxy scavenger and also hydroxyl radicals were removed to a lesser extent (in vitro assays, see above).

The analysis of the mitochondrial membrane potential ($\Delta\Psi_m$) was performed using the fluorescent dye TMRM. The results showed that the lower level (30%) of TMRM fluorescence after VOchlorog treatment is indicative of the depolarization of mitochondrial membrane potential. The nature of apoptotic signals from mitochondria has been well documented [54]. Cytochrome *c* and apoptosis-inducing factor (AIF) are well known as proapoptotic molecules released from the mitochondria. Cytochrome *c* usually is released from the mitochondrial intermembrane space into the cytosol as a consequence of the mitochondrial membrane potential loss. Cytochrome *c* released from the mitochondria forms a complex with procaspase-9 and apoptotic protease-activating factor-1 (Apaf-1), resulting in activation of procaspase-9. Contrarily, AIF condenses chromatin to induce apoptosis without involvement of caspases. Although mechanism of the AIF release from the mitochondria has not been fully understood, the regulatory role of AIF during programmed

Table 5
Effects of chlorogenic acid and VOchlorog on the viability and the possible mechanisms of action on SKBR3, MDAMB231 and T47D human breast cell lines.

	SKBR3		MDAMB231		T47D	
	Chlorogenic acid	VOchlorog	Chlorogenic acid	VOchlorog	Chlorogenic acid	VOchlorog
Percent survival	90%	60%	100%	100%	116%	111%
ROS	NO	NO	NO	NO	NO	NO
TMRM	NO	30% (decrease)	NO	NO	NO	NO
Caspase 3/7	NO	NO	NO	NO	NO	NO
H2AX	NO	25% (increase)	NO	NO	NO	NO
LDH	NO	99% (increase)	NO	NO	NO	NO

High content analysis image assay: reactive oxygen species, ROS were determined using the CMH2DCFDA probe. Mitochondrial membrane potential disruption was detected using TMRM probe. Caspase 3/7 activation was determined using CellEvent™ Caspase 3/7 Green Detection Reagent. Histone H2AX phosphorylation (DNA damage) was determined by an immunohistochemistry method. The measurement of LDH release (plasmatic membrane damage) was performed using the cytotoxicity detection kit (LDH).

cell death has been well documented. AIF is a putative caspase-independent effector of cell death. Similar to cytochrome *c*, AIF is released from the mitochondria in response to death stimuli. On induction of apoptosis, AIF is translocated to the nucleus and causes large-scale DNA fragmentation and chromatin condensation in a caspase-independent manner [55].

Our results suggest that a caspase-independent pathway could be involved in the induction of apoptotic cell death (VOchlorog did not produce caspase 3/7 activation) but $\Delta\Psi_m$ is disrupted. On the other hand, the oxidovanadium(IV) complex induced DNA damage in SKBR3 cell line. In Table 5, it can be seen that the complex produced histone H2AX phosphorylation in response to the induction of DNA double-strand breaks. Lactate dehydrogenase (LDH) is used as a reliable marker to test cytotoxicity, because damaged cells are fragmented completely during the course of prolonged incubation and release of LDH. The release of LDH (99%) in SKBR3 cancer cells may be due to the cytotoxic nature of the VOchlorog and confirms its anti-tumor activity.

According to the observations displayed in Table 5 only VOchlorog produced a significant effect on the SKBR3 cell viability. The mitochondrial membrane potential was disrupted after treatment with 10 μM of oxidovanadium(IV) complex. It can be seen that VOchlorog produced histone phosphorylation and damage in plasmatic membrane. The caspase 3/7 pathway was not activated by the addition of the oxidovanadium(IV) complex, therefore we can conclude that the death mechanistic of this compound is caspase independent.

7. Spectroscopic examination on the transport mechanism with bovine serum albumin

Bovine serum albumin (BSA) has a large variety of physiological functions relating to the binding, transport, and delivery of some substances like fatty acids, porphyrins, bilirubin, and steroids, among others. It is well known that the efficiency of drugs depends on their binding ability. The binding affinity affects the rate at which the drug is released to perform its pharmacological action. The study of the binding ability of drugs to BSA provides information of structural features that determine the therapeutic efficacy of drugs. Hence, the interaction of metal complexes having potential biological activity is converted into a relevant research field in bioinorganic chemistry, inorganic pharmaceutical chemistry and medicinal chemistry.

For that reason, we included the investigation of the interaction of chlorogenic acid and VOchlorog with BSA analyzing by FTIR and fluorescence spectroscopies, the conformational changes of the protein after binding reactions.

7.1. Fluorescence spectra

The conformational changes of BSA were evaluated by the measurement of intrinsic fluorescence intensity of protein before and after addition of drug. Fluorescence measurements give information about the molecular environment in a surrounding area of the chromophore

molecules. Fig. 9 shows the fluorescence quenching spectra of solutions containing BSA at fixed concentration and different concentrations of each of the studied compounds.

The effect of free V(IV)O^{2+} on the fluorescence of BSA was shown in Fig. 9A. The result showed that the increasing concentrations of V(IV)O^{2+} scarcely changed the fluorescence intensity of BSA. It had a slight blue-shift of BSA fluorescence emission maximum wavelength when the solution of V(IV)O^{2+} was added, leading to a 10% quenching of fluorescence at 100 μM and suggesting that the binding is possibly associated with changes in the dielectric environment of at least one of the two indole rings in BSA [56].

Nevertheless the specific binding of chlorogenic acid to serum albumins under physiological conditions has been previously reported [57]. Here we presented the results obtained in our experimental conditions (Fig. 9B). It can be observed that fluorescence was strongly quenched and the fluorescence emission wavelengths of BSA have a red shift after the protein interacted with the drug, most significantly at higher drug concentration. The red shift indicated that the tryptophan residue in protein has been brought to a more hydrophilic environment of the region surrounding the Trp^{214} site [58].

As can be seen from Fig. 9C, the addition of increasing concentrations of VOchlorog caused a progressive reduction of the fluorescence intensity which indicated that the complex also interacted with BSA and only at higher concentration values a slight red shift was observed. This behavior suggested that it was more likely that hydrophobic, electrostatic interactions were involved in its binding process going to the unfolding of the protein [59].

Fluorescence quenching mechanism for chlorogenic acid and VOchlorog were analyzed by using at first the Stern–Volmer equation: $F_0 / F = 1 + K_{sv}[Q]$ (Eq. (1), not shown) and then by the modified Stern–Volmer: $F_0 / F_0 - F = 1 / f_a + 1 / f_a K_{sv}[Q]$ (Eq. (2), inset of Fig. 9B and C); where F_0 and F denote the steady-state fluorescence intensities in the absence and in the presence of the quencher, respectively. K_{sv} is the Stern–Volmer quenching constant, and $[Q]$ is the concentration of the quencher. The curve of $F_0 / (F_0 - F)$ versus $1/[Q]$ should be linear for static quenching [60], in which f_a is the fraction of the initial fluorescence which is accessible to quencher. From this plot (inset of Fig. 9B and C) the f_a and K_{sv} were obtained from the values of intercept and slope, respectively. For chlorogenic acid and VOchlorog, the values of f_a were found to be 1.29 and 1.23 indicating that 77.52% and 81.10% of the total fluorescence of BSA are accessible to the quencher. The Stern–Volmer quenching constant for chlorogenic acid was found to be $K_{sv} = 2.98 \times 10^4 \text{ M}^{-1}$ in concordance with previously reported data [44] and for VOchlorog the K_{sv} constant was $3.76 \times 10^4 \text{ M}^{-1}$. Taking into account the well known relationship between the quenching rate constant of the biomolecule K_q and the dynamic quenching constant K_{sv} ($K_q = K_{sv} / \tau_0$, where τ_0 is the average lifetime of the biomolecule without quencher), and taking into consideration that the fluorescence lifetime of the biopolymer is 10^{-8} s , K_q can be calculated using this equation. The calculated 0.15pt^2 -values were $2.98 \times 10^{12} \text{ M}^{-1} \text{ s}^{-1}$ and $3.76 \times 10^{12} \text{ M}^{-1} \text{ s}^{-1}$, respectively. However, the maximum scatter collision quenching constant K_q of various quenchers with the biopolymer is 2

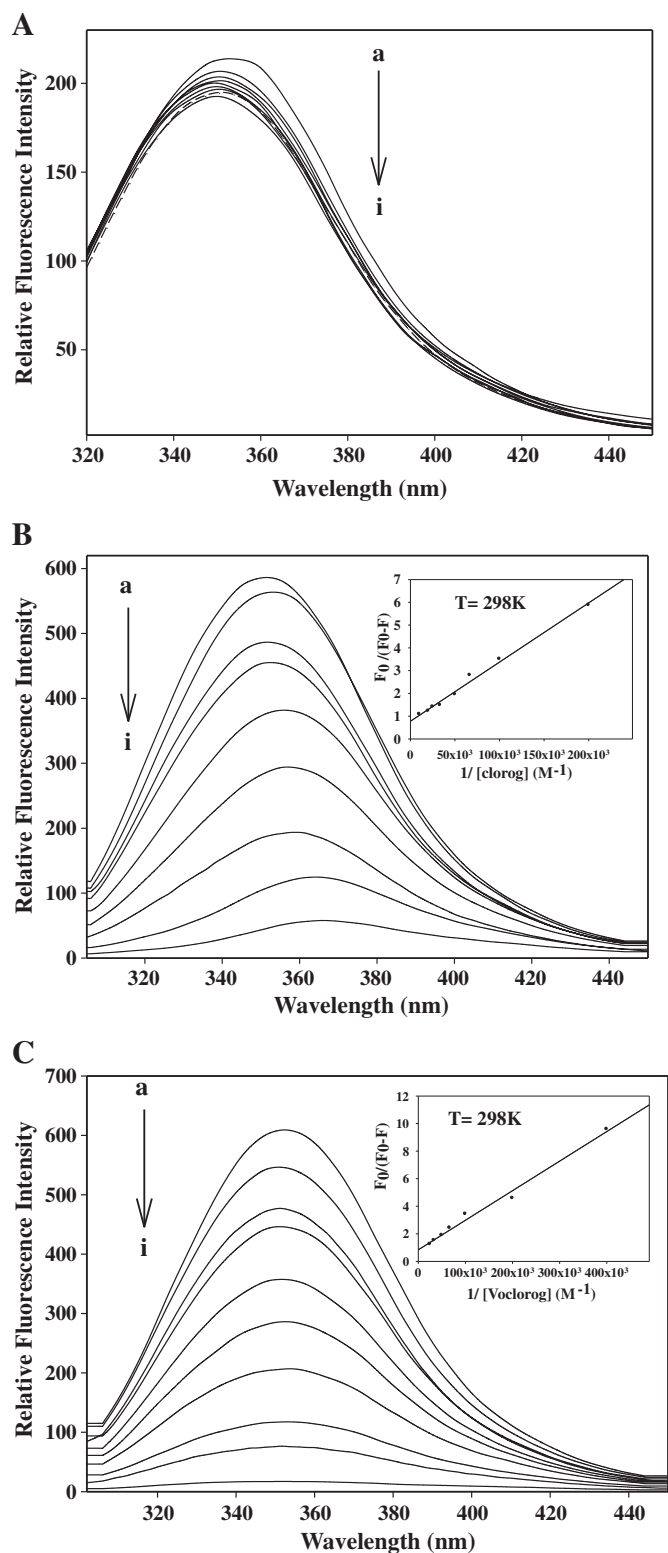


Fig. 9. Fluorescence quenching experiments. Spectra of solutions of BSA at a fixed concentration (6 μM) and different concentrations of each of the compounds. Concentration range: (a) BSA 2% w/w (basal), (b) 2 μM , (c) 5 μM , (d) 10 μM , (e) 15 μM , (f) 20 μM , (g) 30 μM , (h) 40 μM , (i) 50 μM , and (j) 100 μM . (A) V(IV)O_2^+ , (B) chlorogenic acid, and (C) VOchlorog. Inset of panels (B) and (C): modified Stern–Volmer equation. Excitation at 280 nm and emission at 348 nm (25 $^\circ\text{C}$).

$\times 10^{10} \text{ M}^{-1} \text{ s}^{-1}$. Obviously, the rate constant of the protein quenching procedure initiated by chlorogenic acid and VOchlorog is greater than the K_q of the scatter procedure. This means that the quenching is not

initiated by dynamic collision but is from the formation of a complex, which suggests that there was a specific interaction occurring between BSA and the studied compounds.

Analysis of binding equilibria can be obtained using the equation:

$$\log (F_0 - F)/F = \log K_a + n \log [Q] \quad (3)$$

where, in the present case, K_a is the binding constant to a site, and n is the number of binding sites per BSA. According to Eq. (3) the binding constant K_a and the number of binding sites n could be obtained as: $K_a = 3.92 \times 10^6 \text{ M}^{-1}$ and $n = 1.39$ for the ligand and $K_a = 1.19 \times 10^7 \text{ M}^{-1}$ and $n = 1.47$ for the complex. The numbers of binding sites were both about 1.0, which indicated that one binding site is formed between chlorogenic and VOchlorog and BSA, and that these values corresponded with the binding sites with high affinity. The value of binding constant of the ligand to BSA was in the range of 10^3 – 10^6 M^{-1} , which agreed with the common affinities of drugs for serum albumin. On the other hand, VOchlorog, has a K_a value greater than that found for other transition metal complexes of Zn(II) [61], Cu(II) [62] and Fe(III) [63].

7.2. Exploring BSA structure

Attachment of chlorogenic and VOchlorog to BSA affects electrostatic and hydrophobic interactions, producing conformational changes. The induced conformational changes on BSA structure were also established by FTIR spectroscopy. It is well documented that Amide I band (1700 – 1600 cm^{-1}) reflects an almost pure vibrational character that is a well-recognized potential in protein secondary structure studies so that these bands were analyzed. The main spectral features of native BSA are characterized by a strong Amide I band at 1657 cm^{-1} which is indicative of the predominance of the α -helix conformation on BSA secondary structure. Quantitative analysis of the corresponding secondary structures in Amide I region was achieved. For BSA 2% w/w and VOCl_2 –BSA mixture calculations were in accordance with our previous reported data [64]. Each polypeptide conformation could be related to a greater or lesser degree of protein folding. The α -helix conformation is a more compact structure while the random coil conformation is a less compact and more disordered one [65]. In comparison with the BSA native structure [64] the curve-fitting procedure indicated that chlorogenic and VOchlorog species (Table 6) decreased their α -helix content with the minor proportion being to the complex. On the other hand, there is an increment in β -sheets and random coil structures. The reduction observed in α -helix conformation and the significant enhancement in disordered structures in relation to BSA native structure are consistent with the hypothesis of the existence of a strong interaction between these species and BSA being more significant for VOchlorog complex.

These findings together with a higher binding constant would indicate that for VOchlorog the complexation enhances the capacity of

Table 6

FT-IR determination of secondary structure percentages of chlorogenic (0.5 mM)–BSA (2% w/w) and VOchlorog (0.5 mM)–BSA (2% w/w) in Tris–HCl buffer (freeze-dried powdered samples).

Amide I components	Chlorogenic–BSA	VOchlorog–BSA
β -Antiparallel (1675 – 1695 cm^{-1})	16.13 ± 0.30	20.57 ± 0.28
Turns (1666 – 1673 cm^{-1})	9.39 ± 0.15	9.88 ± 0.20
α -Helix (1650 – 1658 cm^{-1})	20.43 ± 0.42	16.76 ± 0.39
Random coil (1637 – 1645 cm^{-1})	9.06 ± 0.23	5.40 ± 0.15
Solvated helix (1625 – 1637 cm^{-1})	11.16 ± 0.25	33.29 ± 0.76
β -Sheets (1613 – 1625 cm^{-1})	33.79 ± 0.76	14.11 ± 0.32

Data represent average obtained from three independent replicates, standard error is indicated.

Band assignment was performed taking into account references [29,30].

interaction with albumin, providing evidence that the complex may be carried by BSA.

8. Conclusions

The studies for the chlorogenic acid/ $V(IV)O^{2+}$ system allow us to propose the formation of a solid complex with a metal-to-ligand 1:1 stoichiometry $Na[VO(chlorog)(H_2O)_3] \cdot 4H_2O$ ($VOchlorog$). It is noteworthy that the synthetic conditions were based on potentiometric studies (species distribution diagrams) and in the EPR analysis. The use of these diagrams and the monitoring of speciation by EPR spectroscopy allowed us to detect the presence of the 1:1 M:L metal-to-ligand species as majority in the synthetic conditions ($pH = 5$) and the 1:2 M:L ratio species at physiological pH conditions. Moreover, elemental analyses and TGA studies confirmed the existence of seven water molecules. The presence of sodium in the complex was confirmed by elemental analyses and by the presence of $NaVO_3$ as final residue of the thermal decomposition (FTIR spectral determination). The vibrational FTIR measurements suggested the lack of coordination of the carboxylate and the carbonyl groups to $V(IV)O^{2+}$ and that the interaction occurs through the deprotonated OH groups of the molecule. The coordination sphere around the metal center was also supported by the EPR data which propose the existence of two ArO^- groups from one ligand and the presence of two water molecules in the equatorial position. The complex behaved as a good antioxidant agent with strongest inhibitory effects towards reactive oxygen species such as $O_2^{\cdot-}$, OH^{\cdot} and ROO^{\cdot} radicals. Moreover, $VOchlorogenic$ exhibits selective cytotoxicity against SKBR3 cancer cell line with a probable “caspase independent” mechanism of action. Albumin interaction experiments demonstrate that there is a great possibility that the complex would be carried by this protein in the biological media. These findings predict the potency of the new compound as a promising metal based drug with antioxidant and anti-cancer properties.

Abbreviations

AAPH	2,2-azobis(2-amidinopropane) dihydrochloride
ABTS	2,2'-azinobis(3-ethylbenzothiazoline-6-sulfonic acid) diammonium salt
ABTS ⁺	2,2'-azinobis(3-ethylbenzothiazoline-6-sulfonic acid) diammonium salt radical cation
BSA	bovine serum albumin
Chlorog	chlorogenic acid
DAPI	4',6'-diamidino-2-phenylindole
DPPH [•]	1,1-diphenyl-2-picrylhydrazyl radical
H2AX	subtype of H2A histone
IC_{50}	50% inhibition concentrations
LDH	lactate dehydrogenase
McCF	McCord–Fridovich
MTT	3-(4,5-methyl-thiazol-2-yl)-2,5-diphenyl-tetrazolium bromide
NBT	nitroblue tetrazolium
PBS	phosphate-buffered saline
PMS	phenazine methosulfate
ROS	reactive oxygen species
SOD	superoxide dismutase
TEAC	Trolox equivalent antioxidant coefficient
TMRM	tetramethyl rhodamine methyl ester
Trolox	6-hydroxy-2,5,7,8-tetramethylchroman-2-carboxylic acid
$VOchlorog$	$Na[VO(chlorog)(H_2O)_3] \cdot 4H_2O$

Acknowledgments

This work was supported by UNLP, CONICET, CICPBA and INNOPROT. AGB and EGF are members of the Carrera del Investigador, CONICET.

PAMW is a member of the Carrera del Investigador CICPBA, Argentina. LN is a fellowship holder from CONICET.

Appendix A. Supplementary data

Supplementary data to this article can be found online at <http://dx.doi.org/10.1016/j.jinorgbio.2014.02.013>.

References

- [1] M.D. dos Santos, P.R. Martins, P.A. dos Santos, R. Bortocan, Y. Iamamoto, N.P. Lopes, *Eur. J. Pharm. Sci.* 26 (2005) 62–70.
- [2] M.N. Clifford, *J. Sci. Food Agric.* 79 (1999) 362–372.
- [3] Y. Kono, S. Sashine, T. Yoneyama, Y. Sakamoto, Y. Matsui, H. Shibata, *Biosci. Biotechnol. Biochem.* 62 (1998) 22–27.
- [4] R.K. Sharma, M.R. Hajaligol, P.A. Martoglio Smith, J.B. Wooten, V. Baliga, *Energy Fuel* 14 (2000) 1083–1093.
- [5] E.M. Marinova, A. Toneva, N. Yanishlieva, *Food Chem.* 114 (2009) 1498–1502.
- [6] J. Bouayed, H. Rammal, A. Dicko, C. Younos, R. Soulimani, *J. Neurol. Sci.* 262 (2007) 77–84.
- [7] Y. Kono, K. Kobayashi, S. Tagawa, K. Adachi, A. Ueda, Y. Sawa, H. Shibata, *Biochim. Biophys. Acta* 1335 (1997) 335–342.
- [8] Y. Sato, S. Itagaki, T. Kurokawa, J. Ogura, M. Kobayashi, T. Hirano, M. Sugawara, K. Iseki, *Int. J. Pharm.* 403 (2011) 136–138.
- [9] S. Rakshit, L. Mandal, B. Chandra Pal, J. Bagchi, N. Biswas, J. Chaudhuri, A. Acharya Chowdhury, A. Manna, U. Chaudhuri, A. Konar, T. Mukherjee, P. Jaisankar, S. Bandyopadhyay, *Biochem. Pharmacol.* 80 (2010) 1662–1675.
- [10] M. Daglia, *Curr. Opin. Biotechnol.* 23 (2012) 174–181.
- [11] Y. Kono, H. Shibata, Y. Kodama, A. Ueda, Y. Sawa, *Biochem. Biophys. Res. Commun.* 217 (1995) 972–978.
- [12] B. McDougall, P.J. King, B.W. Wu, Z. Hostomsky, M.G. Reinecke, W.E. Robinson, *Antimicrob. Agents Chemother.* 42 (1998) 140–146.
- [13] Q.-F. Zhang, Y.-X. Guo, X. Shanguan, G. Zheng, W.-J. Wang, *Food Chem.* 133 (2012) 140–145.
- [14] E.G. Ferrer, P.A.M. Williams PAM, Modification of flavonoid structure by oxovanadium(IV) complexation. Biological effects, in: K. Yamane, Y. Kato (Eds.), *Handbook on Flavonoids: Dietary Sources, Properties and Health Benefits*, Series: Biochemistry Research Trends, Nutrition and Diet Research ProgressN. Nova Science Publishers, 2012, pp. 143–195.
- [15] D.C. Crans, J.J. Smee, E. Gaidamauskas, L. Yang, *Chem. Rev.* 104 (2004) 849–902.
- [16] A. Bishayee, A. Waghay, M.A. Patel, M. Chatterjee, *Cancer Lett.* 294 (2010) 1–12.
- [17] B. Desoize, *Anticancer Res.* 24 (2004) 1529–1544.
- [18] A.M. Evangelou, *Crit. Rev. Oncol. Hematol.* 42 (2002) 249–265.
- [19] R.K. Narla, Y. Dong, O.J. D'Cruz, C. Navara, F.M. Uckun, *Clin. Cancer Res.* 6 (2000) 1546–1556.
- [20] L.G. Naso, E.G. Ferrer, N. Butenko, I. Cavaco, L. Lezama, T. Rojo, S.B. Etcheverry, P.A.M. Williams, *J. Biol. Inorg. Chem.* 16 (2011) 653–668.
- [21] L. Naso, E.G. Ferrer, L. Lezama, T. Rojo, S.B. Etcheverry, P.A.M. Williams, *J. Biol. Inorg. Chem.* 15 (2010) 889–902.
- [22] S.B. Etcheverry, E.G. Ferrer, L. Naso, J. Rivadeneira, V. Salinas, P.A.M. Williams, *J. Biol. Inorg. Chem.* 13 (2008) 435–447.
- [23] E.G. Ferrer, M.V. Salinas, M.J. Correa, L. Naso, D.A. Barrio, S.B. Etcheverry, L. Lezama, T. Rojo, P.A.M. Williams, *J. Biol. Inorg. Chem.* 11 (2006) 791–801.
- [24] R.S. Ray, B. Ghosh, A. Rana, M. Chatterjee, *Int. J. Cancer* 120 (2006) 13–23.
- [25] P. Noblía, M. Vieites, B.S. Parajón-Costa, E.J. Baran, H. Cerecetto, P. Draper, M. González, O.E. Piro, E.E. Castellano, A. Azqueta, A. López de Ceráin, A. Monge-Vega, D. Gambino, *J. Inorg. Biochem.* 99 (2005) 443–451.
- [26] P.J. Scrivens, M.A. Alaoui-Jamali, G. Giannini, T. Wang, M. Loignon, G. Batist, V.A. Sandor, *Mol. Cancer Ther.* 2 (2003) 1053–1059.
- [27] R.K. Narla, C.-L. Chen, Y. Dong, F.M. Uckun, *Clin. Cancer Res.* 7 (2001) 2124–2133.
- [28] S.B. Etcheverry, D.A. Barrio, J. Zinczuk, P.A.M. Williams, E.J. Baran, *J. Inorg. Biochem.* 99 (2005) 2322–2327.
- [29] A.T. Tu, *Raman spectroscopy in biology, Principals and Applications*, John Wiley & Sons, Inc., New York, 1982, pp. 65–116, (and references therein).
- [30] D.M. Byler, H. Susi, *Biopolymers* 25 (1986) 469–487.
- [31] S. Durot, C. Policar, F. Cisnetti, F. Lambert, J.-P. Renault, G. Pelosi, G. Blain, H. Korri-Youssoufi, J.P. Mahy, *Eur. J. Inorg. Chem.* 14 (2005) 3513–3523.
- [32] R. Swislocka, *Spectrochim. Acta, Part A* 100 (2013) 21–30.
- [33] Y. Allegretti, E.G. Ferrer, A.C. González Baró, P.A.M. Williams, *Polyhedron* 19 (2000) 2613–2619.
- [34] M. Menelaou, C. Mateescu, H. Zhao, N. Lalioti, A. Salifoglou, *Polyhedron* 28 (2009) 883–890.
- [35] J.P. Cornard, C. Lapouge, *J. Phys. Chem. A* 108 (2004) 4470–4478.
- [36] S.B. Etcheverry, D.A. Barrio, A.M. Cortizo, P.A.M. Williams, *J. Inorg. Biochem.* 88 (2002) 94–100.
- [37] A.E. Martell, R.J. Motekaitis, *Determination and Use of Stability Constants*, 2nd ed. VCH Publishers Inc., New York, 1992.
- [38] J.P. Cornard, C. Lapouge, L. Dangleterre, C. Allet-Bodelot, *J. Phys. Chem.* 112 (2008) 12475–12484.
- [39] H. Esbak, E.A. Enyed, T. Kiss, Y. Yoshikawa, H. Sakurai, E. Garribba, D. Rehder, *J. Inorg. Biochem.* 103 (2009) 590–600.

- [40] N.D. Chasteen, Vanadyl(IV) EPR spin probes, in: J. Lawrence, L.J. Berliner, J. Reuben (Eds.), *Biological Magnetic Resonance, Inorganic and Biochemical Aspects*, vol. 3, Plenum, New York, 1981, pp. 53–119, (chapter 2).
- [41] J.P. Cornard, C. Lapouge, L. Dangleterre, C. Allet-Bodelot, *J. Phys. Chem. A* 112 (2008) 12475–12484.
- [42] M.L. Adams, B. O'Sullivan, A.J. Downard, K.J. Powell, *J. Chem. Eng. Data* 47 (2002) 289–296.
- [43] H.S. Mahal, S. Kapoor, A.K. Satpati, T. Mukherjee, *J. Phys. Chem. B* 109 (2005) 24197–24202.
- [44] J. Tabart, C. Kevers, J. Pincemail, J.O. Defraigne, J. Dommes, *Food Chem.* 113 (2009) 1226–1233.
- [45] N. Nakatani, S. Kayano, H. Kikuzaki, K. Sumino, K. Katagiri, T. Mitani, *J. Agric. Food Chem.* 48 (2000) 5512–5516.
- [46] M. Ohnishi, H. Morishita, S. Toda, Y. Yase, R. Kido, *Phytochemistry* 47 (1998) 1215–1218.
- [47] J. Shi, J. Gong, J. Liu, X. Wu, Y. Zhang, *LWT-Food Sci. Technol.* 42 (2009) 477–482.
- [48] Z. Xiang, Z. Ning, *LWT* 41 (2008) 1189–1203.
- [49] A. Jemal, F. Bray, M.M. Center, J. Ferlay, E. Ward, D. Forman, *Cancer J. Clin.* 61 (2011) 69–90.
- [50] E.R. dos Santos, M.A. Mondelli, L.V. Pozzi, R.S. Corrêa, H.S. Salistre-de-Araújo, F.R. Pavan, C.Q.F. Leite, J. Ellena, V.R.S. Malta, S.P. Machado, A.A. Batista, *Polyhedron* 51 (2013) 292–297.
- [51] S. Deepthia, R. Trivedia, P. Sujitha, C.G. Kumar, B. Sridharc, S.K. Bhargavad, *J. Chem. Sci.* 124 (2012) 1405–1413.
- [52] J. Ruiz, C. Vicente, C. Haro, D. Bautista, *Inorg. Chem.* 52 (2013) 974–982.
- [53] E. de Paula Silveira-Lacerda, C.A. Sam Tiago Vilanova-Costa, A. Hamaguchi, L.A. Pavanin, L.R. Goulart, M.I. Homsí-Brandenburgo, W. Batista dos Santos, A. Martins Soares, A. Nomizo, *Biol. Trace Elem. Res.* 135 (2010) 98–111.
- [54] A.G. Porter, R.U. Jaënicke1, *Cell Death Differ.* 6 (1999) 99–104.
- [55] Y.H. Kang, M.J. Yi, M.J. Kim, M.T. Park, S. Bae, C.M. Kang, C.K. Cho, I.C. Park, M.J. Park, C.H. Rhee, S. Hong, H.Y. Chung, Y.S. Lee, S.J. Lee, *Cancer Res.* 64 (2004) 8960–8967.
- [56] J. Tiana, J. Liua, X. Tiana, Z. Hua, X. Chena, *J. Mol. Struct.* 691 (2004) 197–202.
- [57] Y.-J. Hu, C.-H. Chen, S. Zhou, A.-M. Bai, Y.-O. Yang, *Mol. Biol. Rep.* 39 (2012) 2781–2787.
- [58] Y.-J. Hu, Y. Liu, Z.-B. Pia, S.-S. Qu, *Bioorg. Med. Chem.* 13 (2005) 6609–6614.
- [59] S. Cao, X. Jiang, J. Chen, *J. Inorg. Biochem.* 104 (2010) 146–152.
- [60] N.M. Urquiza, L.G. Naso, S.G. Manca, L. Lezama, T. Rojo, P.A.M. Williams, E.G. Ferrer, *Polyhedron* 31 (2012) 530–538.
- [61] M. Gharagozloua, D.M. Boghaei, *Spectrochim. Acta, Part A* 71 (2008) 1617–1622.
- [62] Y.-Z. Zhang, X.-P. Zhang, H.-N. Hou, J. Dai, Y. Liu, *Biol. Trace Elem. Res.* 121 (2008) 276–287.
- [63] H. Zhang, Y. Wang, Z. Fei, L. Wu, Q. Zhou, *Dyes Pigments* 78 (2008) 239–247.
- [64] E.G. Ferrer, A. Bosch, O. Yantorno, E.J. Baran, *Bioorg. Med. Chem.* 16 (2008) 3878–3886.
- [65] E.G. Ferrer, A.V. Gómez, M.C. Añón, M.C. Puppo, *Spectrochim. Acta, Part A* 79 (2011) 278–281.